# Chemical Genetic Screen Identifies PSD3 as a Direct Substrate of NUAK1 that Regulates Dendritic Spine Maturation

Josilyn R. Sejd[1], Daphnée M. Marciniak[1], Moira A. Cornell[1], Angel Sondhi[1], Shao-En Ong[1] and Smita Yadav[1,2*]

[1]Department of Pharmacology, University of Washington, Seattle, United States.
[2]Institute of Stem Cell and Regenerative Medicine, Seattle, United States
* Corresponding author

## Abstract

Novel *(nua)* Kinase 1 *(NUAK1)* encodes a serine-threonine protein kinase, mutations in which are associated with autism spectrum disorder. Direct phosphorylation targets of NUAK1 have been elusive hindering mechanistic understanding of its role in brain development. Here, we characterize autism-associated NUAK1 variants and show their differential impact on catalytic activity and subcellular distribution. We engineered ATP-analog sensitive NUAK1 and utilized its specificity towards bulky analogs to identify over 30 hitherto unknown direct phosphorylation targets of NUAK1. We demonstrate that Pleckstrin Homology and Sec7-domain containing protein 3 (PSD3) is a *bona fide* phosphorylation target of NUAK1. A guanine exchange factor (GEF) for ARF6 GTPase, PSD3 is phosphorylated by NUAK1 at S476. Expression of phosphodeficient PSD3 leads to aberrant activation of ARF6 and generation of $PI(4,5)P_2$ that accumulates in intracellular vesicles. In neurons, phosphomutant PSD3 leads to enhanced spine maturation in an ARF6 dependent fashion. This study reveals direct neuronal substrates of an autism risk gene NUAK1, and delineates a mechanism by which PSD3 phosphorylation regulates ARF6 activation and spine maturation.

## Introduction

NUAK1 is a serine threonine protein kinase that belongs to the AMP-activated protein kinase (AMPK) family[1]. Despite the association of NUAK1 with pathophysiology of autism spectrum disorder[2,3], neurodegenerative disorder[4–6], fibrosis[7,8], immune dysfunction[9], and cancer[10–12], our understanding of this enigmatic kinase has been limited. Several factors have hindered progress in understanding the physiological function of NUAK1 in normal and disease states. NUAK1 knockout mice are embryonically lethal[13], precluding investigation of its physiological function. Moreover, both overexpression and loss of function of NUAK1 are associated with pathogenesis suggesting the importance of its regulated activity. For example, high NUAK1 expression is associated with reduced survival in pancreatic ductal adenocarcinoma and colorectal cancers[9,12]. It is also upregulated in multiple fibrotic tissues in humans, and NUAK1 inhibition in mice attenuates fibrosis[7,8,14]. NUAK1 stabilizes microtubule binding protein tau, and in a tauopathy mouse model its deletion protects against neurodegeneration[5]. In contrast, loss of NUAK1 in the brain causes defects in axonal development and heterozygous NUAK1 knockout mice exhibit social behavior deficits[15,16]. The fact that physiological phosphorylation targets of NUAK1 with a few exceptions have not been identified, has constrained understanding of NUAK1 function in normal and disease states.

The canonical isoform of human NUAK1 contains 661 amino acids with an N-terminal kinase domain and a largely disordered C-terminal region. Most studied in context of tumor suppression and cell proliferation[10,17–19], NUAK1 activity is regulated by LKB1 and NDR2 phosphorylation at the activation loop residue T211[20,21]. Phosphorylation by AKT at S600 has been shown to further increase the catalytic activity of NUAK1[22]. The LKB1-NUAK1 mediated signaling controls cell adhesion through regulation of myosin phosphatase complexes[17]. Three Gly-Iso-Leu-Lys (GILK) motifs in NUAK1 mediate its interaction with phosphatase complex MYPT1-PP1β that controls cell adhesion through regulation of myosin light chain[17]. An alternative pathway for NUAK1 phosphoregulation mediated by calcium-dependent activation of PKCα has been implicated in cancer cells lacking LKB1[23,24], highlighting several routes for achieving NUAK1 activation in distinct cellular context. Greater complexity to NUAK1 signaling arises from distinct subcellular compartments in which NUAK1 has been reported to function. A bipartite nuclear localization signal shuttles NUAK1 into the nucleus, with oxidative stress increasing its nuclear transport[25]. In cancer cell lines, NUAK1 appears to be predominantly nuclear, localized within nuclear speckles where it plays an important role in regulating splicing[24]. Therefore, in the cytoplasm, NUAK1 controls the function of PP1 complex by phosphorylating the MYPT1

regulatory subunit, while in the nucleus NUAK1 interacts with PNUTS/PPP1CB complexes through phosphorylation of PNUTS to regulate cotranscriptional splicing[17,24].

NUAK1 function and signaling in the brain is less understood. Highly expressed in the central nervous system, NUAK1 has been shown to be important for axonal and dendrite development[15,16,26,27]. It is clear that catalytic activity of NUAK1 is essential for its function in the neuronal development. For example, heterozygous NUAK1 knockout mice exhibit impaired axon elongation which can be rescued by expression of WT NUAK1, but not by kinase dead NUAK1[16]. Further, small molecule kinase inhibitors against NUAK1 impair both axon and dendritic development[26]. However, mechanisms through which NUAK1 mediated phosphorylation promotes neuronal development are unknown largely because its direct phosphorylation targets in the brain have not been identified. Further, whether autism associated NUAK1 variants impact its catalytic activity have not been tested.

In our study, we biochemically characterized NUAK1 autism-associated variants and show their differential impact on catalytic function and subcellular localization. Given the importance of its kinase activity and dearth of mapped NUAK1 neuronal substrates, we employed an unbiased chemical-genetic strategy to identify direct phosphorylation targets of NUAK1 in the mouse brain. We reveal neuronal substrates of NUAK1 kinase that span cellular processes of endocytosis, splicing, axon development, dendritic growth and synaptogenesis. From these candidate substrate hits, we demonstrate that PSD3, a nucleotide exchange factor for the small GTPase ARF6, is a *bona fide* substrate of NUAK1. Through a combination of in vitro biochemical assays, phosphomutant analyses in neurons and super resolution imaging, we have uncovered an essential role of NUAK1 mediated phosphorylation of PSD3 that controls ARF6 and PI(4,5)P2 dependent endocytic trafficking and dendritic spine maturation.

# Results

### Autism-Associated NUAK1 Variants Perturb Kinase Activity and Subcellular Distribution

NUAK1 has previously been reported to have differential subcellular localization to either the nucleus and/or cytosol depending on cell/tissue type and nutrient conditions[8]. To study the role of NUAK1 in brain development, we first investigated its localization in neuronal cells. Rat embryonic hippocampal neurons were fixed at 14 days *in vitro* (DIV) and then immunostained with an antibody against NUAK1 to visualize neuronal localization of endogenous NUAK1, along with an antibody against the dendrite marker MAP2 *(Fig.1a)*. We found that endogenous NUAK1 is

95 localized to the cytosol within the soma, dendrites, and axon with no observable nuclear
96 enrichment within neurons (Fig.1a). In human brain, the Human Brain Transcriptome
97 database[28] shows NUAK1 is also highly expressed in early development across all measured
98 brain regions (NCX, HIP, AMY, STR, MD, CBC), and its expression persists into adulthood
99 (Fig.1b). Similarly, NUAK1 is highly expressed in neurons within the cortex, hippocampus, and
100 cerebellum as seen in ISH staining data by the Allen Brain Atlas (*Fig.1c*). Similar to endogenous
101 NUAK1, exogenously expressed GFP-tagged NUAK1 was also largely cytosolic. We next
102 interrogated the impact of NUAK1 autism-associated variants on its catalytic activity and neuronal
103 localization. Three NUAK1 variants have been reported to date; missense mutation Q161E within
104 the kinase domain, premature truncation mutant Q433*, and missense mutation A653V in the C-
105 terminal tail[29–31] (Fig.1d). Evolutionary analyses with ConSurf[32] revealed conservation of the
106 residues mutated in missense mutations. The Q161 residue shows 100% conservation across
107 150 species and there was 98% conservation of residue A653, with only the small amino acids
108 glycine or serine observed at this position (Fig.1e). Alphafold3[33,34] model of NUAK1 predicts A653
109 residue to be located in an alpha helix. We used HeliQuest[35] to probe the nature of this alpha
110 helix and found that residues 640-661 formed an amphipathic helix (Fig.S1a-b), with A653 located
111 in the hydrophobic face (Fig.1d and 1f).
112
113 Next, we tested whether autism-associated NUAK1 variants impacted its catalytic activity
114 by performing an *in vitro* kinase activity assay[36]. Briefly, GFP-tagged NUAK1 variants were
115 expressed in HEK293T cells, followed by lysis, immunoprecipitation, and incubation with $Mg^{2+}$
116 and ATP. We observed robust autophosphorylation with WT NUAK1, which was lost with the
117 catalytic lysine mutation K84M kinase dead (KD) mutation (Fig.1g-h). We observed a greater that
118 80-fold reduction in catalytic activity with the Q161E mutant, while the Q433* and A653V
119 mutations had unchanged kinase activity relative to WT NUAK1 (Fig.1g-h). To evaluate the impact
120 of NUAK1 variants on its subcellular distribution in neurons, we expressed GFP-tagged NUAK1
121 mutants in hippocampal neurons and found that while the Q161E and A653V variants had similar
122 localization to WT, expression of NUAK1 truncation variant Q433* dramatically induced nuclear
123 localization (Fig.1i). While the A653V mutation did not impact catalytic activity or nuclear
124 localization in neurons, we sought to ascertain if any other functions of this protein were impacted
125 by this mutation. While neuronal NUAK1 is excluded from the nucleus, NUAK1 in mitotically active
126 cells has well-established kinase activity-dependent roles in regulation of splicing[24,37]. WT NUAK1
127 has been shown to colocalize with SC35, a marker of spliceosomes, in the nucleus in various
128 contexts[24,37]. We expressed GFP-tagged NUAK1 (WT, Q161E, Q433* and A653V) in human

129 WTC11 (Corielle) iPSC-derived neural progenitor cells (NPCs) (Fig.S1b). In NPCs, WT NUAK1
130 localizes to the cytosol and nucleus, and is also enriched in nuclear speckles. In contrast,
131 truncation mutant Q433* NUAK1 is entirely absent from the cytosol and instead enriched in
132 nuclear speckles positive for SC35. Remarkably, the kinase deficient mutant Q161E NUAK1 does
133 not show colocalization with SC35 positive nuclear speckles. While catalytically active, in NPCs
134 the mutant A653V NUAK1 shows nuclear and cytosolic localization, but is absent from SC35
135 positive nuclear speckles (Fig.S1a). These experiments suggest that NUAK1 mutations might
136 lead to decreased phosphorylation of its neuronal substrates either through deficits in its catalytic
137 function (Q161E) or aberrant shift in its distribution between the cytoplasm to the nuclear speckles
138 (A653V and Q433stop).
139
140 **Chemical-Genetic Screen for Identification of NUAK1 direct neuronal targets**
141 NUAK1 phosphorylation targets in the developing brain have not been identified. We
142 employed a chemical-genetics approach[38–41] where we engineered a bulky ATP analog sensitive
143 (AS) NUAK1 that uniquely thiophosphorylates substrates that are covalently captured by
144 iodoacetamide beads and then identified by mass spectrometry. The advantages of this method
145 are that first, it uniquely identifies direct phosphorylation targets of the kinase of interest, and
146 second, the phosphorylation site on the substrate is revealed that can be then modified to study
147 physiological impact of phosphorylation. To engineer the AS-NUAK1 kinase, we mutated the
148 conserved gatekeeper residue M132 in the kinase domain of NUAK1 (Fig.2a) to a smaller amino
149 acid Alanine or Glycine. With the enlarged hydrophobic nucleotide binding pocket, the engineered
150 AS-NUAK1 can utilize $N^6$-substituted bulky ATPɣS molecules to thiophosphorylate its substrates.
151 As a negative control, we also generated kinase dead (KD) NUAK1 with a Lys84Met (K84M)
152 mutation, abolishing the conserved catalytic lysine residue that is responsible for coordinating the
153 ɣ-phosphate of ATP. We bacterially purified the kinase domain of NUAK1 (residues 1-433) with
154 either active wildtype (WT), kinase-dead (K84M), and analog sensitive (M132G) mutations
155 (Fig.S2a-c). We next combinatorially tested different NUAK1 AS mutants and bulky ATP analogs
156 and determined that $N^6$-furfuryl-ATPɣS is optimally utilized by M132G NUAK1 for phosphorylation
157 but not by WT NUAK1 (Fig.2b-c). We confirmed that full-length NUAK1 M132G shows preferential
158 utilization of $N^6$-furfuryl-ATPɣS using full-length HA-NUAK1 immunoprecipitated from HEK293T
159 cells (Fig.S2d-e).
160
161 Since motifs outside the NUAK1 kinase domain such as the “Gly-Iso-Leu-Lys” (GILK) motif
162 are important for substrate binding[4,16], we utilized full-length AS-NUAK1 (M132G) to identify

163 thiophosphorylated substrates from mouse brain lysate. We affinity purified full-length AS-
164 NUAK1(M132G) and kinase-dead NUAK1(K84M) from HEK293T cells using HA-conjugated
165 beads and incubated them with mouse brain lysate in the presence of furfuryl ATPɣS (Fig.2d).
166 Compared to the lysate only or kinase dead controls, we observed robust signal for
167 thiophosphorylated substrates identified by a phosphothioester antibody in the AS samples but
168 not in the KD or lysate only samples. After validating that full-length HA-NUAK1 AS is able to
169 effectively phosphorylate substrates using furfuryl ATPɣS, we scaled up our system for mass
170 spectrometry analysis. Immunoprecipitated NUAK1 was incubated with mouse brain lysate and
171 furfuryl ATPɣS to allow AS-NUAK1 to thiophosphorylate its substrates. Samples were then
172 denatured with urea, reduced with TCEP, and digested to generate peptides. The resulting
173 thiopeptides were then captured on iodoacetamide resin and treated with oxone to specifically
174 elute peptides containing a thiophosphate moiety, while cysteine (thiol) containing peptides were
175 retained on beads. Eluted phosphopeptides were separated using liquid chromatography and
176 analyzed using mass spectrometry (Fig.2e).
177
178 **Identification of NUAK1 Consensus Sequence and Direct Neuronal Substrates**
179 Mass spectrometry analyses of five replicate samples revealed 972 total phosphopeptides. Our
180 criteria for narrowing candidate hits to be further tested as a *bona fide* substrate of NUAK1
181 following the chemical genetic screen was that the substrate appears in at least three out of five
182 AS replicates and was absent in (0/5) all kinase dead (KD) replicates. From our list of 972 total
183 phospho-serine and phospho-threonine peptides, 31 occurred in at least 3/5 AS replicates and
184 were absent in all 5 KD samples. These 31 potential NUAK1 substrate proteins were analyzed
185 for their cellular role(s) which binned into the following categories: endocytic recycling, splicing,
186 cytoskeletal reorganization, as well as axonal, dendritic, and synaptic development (Fig.3a).
187 Proteins were assigned to one or more categories based on their previously established roles in
188 each cellular process and color coded with either a single color or a gradient of 2-4 colors to
189 indicate their pleiotropic functions (Fig 3a). We used the sequence of these 31 peptides to
190 generate a sequence logo using Phosphosite Plus to show the preferred phosphorylation motif of
191 NUAK1 in our mass spectrometry experiment (Fig.3b). Next, we further shortlisted candidates
192 where the phosphosite sequence fit the experimentally determined NUAK1 stringent consensus
193 sequence of a basic residue (R/K) at the -3 position[42]. Out of the 31 phosphopeptides, 17 fit the
194 stringent consensus of a basic residue at the -3 position (Fig.3c). The substrate phosphopeptides
195 are color coded based on how well the residue fits our optimal NUAK1 phosphorylation motif at
196 positions -5 and +4 (purple), basic residues at positions -4, -3 (cyan), and preferred residue serine

197 at -2 position (chartreuse). The central phosphoacceptor at position 0 is colored in dark green for
198 serine which is preferred over threonine (light green) (Fig.3c). The function and subcellular
199 localization of the 17 putative NUAK1 substrates is listed (Fig.3c) and both nuclear and cytosolic
200 proteins were identified in the chemical genetic screen.
201
202 **PSD3 is a Bona Fide Substrate of NUAK1 Kinase**
203 We next focused on our top candidate in the screen for NUAK1 substrates which was Pleckstrin
204 Homology Domain and SEC7 domain-containing protein 3 (PSD3). A multidomain protein, PSD3
205 consists of a Pleckstrin Homology (PH) domain which binds specifically to phospholipid PI(4,5)$P_2$
206 and a SEC7 domain that acts as an guanine exchange factor (GEF) for small GTPase ARF6[43,44].
207 A coiled coil (CC) region following the PH domain enhances membrane association of the PH
208 domain and has been shown to bind actin[45,46]. These 3 functional domains are present in the
209 alternatively spliced human isoforms of PSD3 (Fig.4a), the canonical isoform 1 with 1048 amino
210 acids (Uniprot #Q9NYI0), isoform 2 with a single amino acid deletion with 1047 amino acids
211 (Uniprot #Q9NYI0-2), and isoform 3 which has 513 amino acids (Uniprot #Q9NYI0-3). The
212 putative NUAK1 phosphorylation site is present in the CC region shared by all three isoforms
213 (Fig.4a). Previous studies have shown that the predominant isoform of PSD3 expressed in the
214 mouse brain is 56kD, which corresponds to isoform 3 [45,47]. PSD3 isoform 3 amino acids 12-513
215 are identical to the C terminal region of PSD3 isoform 1, with only the first 11 amino acids of
216 isoform 3 differing. We utilized ConSurf[32] to perform evolutionary conservation analysis, which
217 revealed that the C-terminus of PSD3 is highly conserved, specifically around the PH, Sec7, and
218 CC domains. Further the phosphosite S476 and the motif surrounding it are extremely conserved
219 (Fig.4b and Fig.S3a). Because our MS-identified phosphosite is located within the evolutionarily
220 conserved C-terminus of both isoforms, we elected to utilize the more abundant shorter isoform
221 3 for further analyses.
222
223 To assess whether affinity purified human PSD3 was phosphorylated by NUAK1, we
224 immunoprecipitated V5-tagged PSD3-WT or phosphomutant V5-PSD3-S476A from HEK293T
225 cells and incubated them with purified NUAK1-WT or NUAK1-KD in an in vitro kinase reaction
226 with ATP. We observed robust phosphorylation of WT PSD3 by WT NUAK1, which was completely
227 lost in the PSD3 S476A mutant (Fig.4c-d). We next determined whether NUAK1 and PSD3
228 interacted with each other. In an affinity pulldown assay with HA-beads, PSD3 was co-
229 immunoprecipitated by HA-tagged NUAK1 but not in the control condition (Fig.4e-f). Similarly,
230 HA-NUAK1 was co-immunoprecipitated by V5-PSD3 (Fig.4g-h), demonstrating that PSD3 and

231 NUAK1 are interacting proteins. To ensure that a co-immunoprecipitating kinase was not
232 responsible for phosphorylating PSD3, we confirmed that bacterially expressed and purified
233 NUAK1 and PSD3 would be sufficient to reconstitute the phosphorylation. We expressed and
234 purified the GST-tagged C-terminal tail of PSD3 which is identical in isoforms 1 and 3 (amino
235 acids 378-513, isoform 3/amino acids 912-1048, isoform 1) encompassing the coiled coil domain
236 and C-terminal tail, and henceforth referred to as 'PSD3-CC-Tail' (Fig.S2a-c). Incubation of
237 purified NUAK1 WT with PSD3-CC Tail in a kinase activity buffer led to phosphorylation of PSD3-
238 CC-Tail which was abolished in the PSD3 S476A mutant. No phosphorylation was observed as
239 expected with the kinase dead NUAK1 (Fig.4i and 4j).
240
241 Next, we used Alphafold3 structure prediction to understand the mechanism through which
242 NUAK1 binds its substrates. First, we performed a prediction of NUAK1 in complex with its known
243 substrate MYPT1, along with the requisite adaptor Protein Phosphatase 1 beta (PP1β)[48]. In this
244 structure, the region of MYPT1 from amino acids 435-455, centered around the phosphosite at
245 S445, docks into the kinase domain of NUAK1, which is shown as an electrostatic surface model
246 (Fig.4k). The phospho-acceptor S445 is located adjacent to the binding site for ATP, while basic
247 residues at the -3 and -4 position bind to acidic patches in the NUAK1 kinase domain. The
248 aliphatic isoleucine residues at -5 and +4 positions in MYPT1 dock into small pockets within the
249 NUAK1 kinase domain. To determine whether NUAK1 had a similar binding mode towards the
250 PSD3 phosphosite, we next modeled NUAK1 in complex with full length PSD3 isoform 1 (Fig.4l).
251 Here, the region surrounding the PSD3 S1011(isoform1)/S476(isoform3) phosphosite docks into
252 the catalytic cleft of NUAK1, in a manner highly similar to MYPT1. The phospho-acceptor
253 S1011/S476 of PSD3 is docked directly next to the ATP-binding site, and the basic residues at
254 positions -4 and -3 are aligned with the acidic patches of the NUAK1 kinase domain. Finally, the
255 aliphatic leucine residues at positions -5 and +4 fit into the pockets in the NUAK1 kinase domain
256 in a similar manner to the respective residues in MYPT1. Altogether, our computational modeling
257 highlights the similarity of the binding conformation of NUAK1 towards known substrate MYPT1
258 and PSD3 discovered in our chemical genetic screen.
259
260 **NUAK1 Phosphorylation of PSD3 Regulates Dendritic Spine Maturation**
261 PSD3 is widely expressed in the central nervous system both during and after developmental
262 time periods. In mouse brain, the highest expression is within the hippocampus and cerebral
263 cortex (Fig.5a), while in human brain PSD3 expression is broad including hippocampus, cortex,
264 striatum and cerebellum. PSD3 expression increases during embryonic brain development,

265 peaks at birth and is maintained at high levels throughout the human lifespan (Fig.5b). PSD3 is a
266 guanine exchange factor specifically for small GTPase ARF6[44], which has important roles in
267 dendritic spine development[49,50]. To determine how NUAK1-mediated PSD3 phosphorylation
268 impacts neuronal development, we transfected DIV12 rat hippocampal neurons with membrane
269 marker myr-tdTomato with either GFP-tagged wildtype PSD3 or the S476A phosphomutant and
270 imaged at DIV14. WT-PSD3 localized throughout the neuron including soma, dendrites, axons
271 and was particularly enriched in mushroom-shaped spines (Fig.5c-d). Notably, we observed that
272 neurons expressing the phosphomutant S476A-PSD3 showed significantly increased enrichment
273 of PSD3 within dendritic spines concomitant with increased number of mushroom spines (Fig.5c
274 and 5d). Percent dendritic spines enriched in PSD3 increased from a mean of 33.8% (n=16 from
275 three experiments) in WT-PSD3 expressing neurons to 63.8% (n=17 from three experiments,
276 $p<0.0001$) in neurons expressing the S476A phosphomutant (Fig.5e). To further analyze the
277 impact of PSD3 phosphorylation on dendritic protrusions, we binned protrusions into four classes:
278 stubby, thin, filopodia and mushroom. While there were no significant differences in the percent
279 of stubby and thin protrusions, the filopodial protrusions decreased from 13.9% to 7.5% in
280 neurons expressing the phosphomutant PSD3 S476A (n=56 neurons from three experiments,
281 SEM=1.33, $p<0.05$) and mushroom spines increased from 36.1% in WT (n=65, SEM=2.08) to
282 48% in S476A mutant expressing neurons (n=56, SEM=2.0, $p<0.0001$) (Fig.5f). No significant
283 differences were observed in total protrusions between the wildtype and S476A mutant PSD3
284 expressing neurons (Fig.5g). These results suggest that NUAK1 mediated phosphorylation of
285 PSD3 at S476 does not impact formation of new protrusions but rather controls the maturation of
286 filopodial protrusions into mature mushroom shaped spines enriched in PSD3.
287
288 **Phosphomutant PSD3 S476A Disrupts ARF6 Mediated Endocytosis**
289 Localization of PSD3 to the plasma membrane is required for conversion of GDP-bound ARF6 to
290 active GTP-bound ARF6. The C-terminal tail of PSD3 containing both the PH domain and the
291 coiled-coils is required for its plasma membrane association[45]. Since S476, the NUAK1
292 phosphosite on PSD3 lies in the C terminal tail, we tested whether PSD3 phosphorylation
293 regulates ARF6 localization or activation. Expression of GFP-tagged wildtype PSD3 along with
294 mScarlet-tagged wildtype ARF6, led to the recruitment to active ARF6 to the membrane (Fig.6a,
295 top row), while expression of catalytically dead PSD3 mutant E114K, as expected, was unable to
296 recruit and activate ARF6 (Fig.6a, second row). Expression of phosphomutant PSD3 recruited
297 ARF6 to the plasma membrane but led to an aberrant accumulation of large vacuole-like
298 intracellular vesicles positive for both ARF6 and PSD3 (Fig.6a, third row). Since constitutively

active ARF6 mutant Q67L leads to similar accumulation of GTP-bound ARF6 that is unable to recycle back, we hypothesized that S476A phosphomutant PSD3 causes aberrant ARF6 activation or prevented the conversion of ARF6 GTP back to its GDP form. To test this hypothesis, we tested whether dominant negative ARF6 mutant T44N would rescue the effect of PSD3 S476A mutant. Indeed, co-expression of PSD3 S476A along with ARF6 T44N did not cause internal accumulation of PSD3 and ARF6 positive vesicles (Fig.6a, bottom row). Area of internalized PSD3/ARF6 positive vesicles increased from 9.6% in WT-PSD3/WT-ARF6 expressing cells to 20.9% in S476A-PSD3/WT-ARF6 expressing cells (n=26, $p<0.005$) (Fig.6b). Expression of S476A-PSD3 with DN-ARF6 lead to almost complete rescue to 2.2% (n=20, $p<0.0001$) similar to the inactive E114K PSD3 expression. GTP-bound ARF6 activates phosphatidylinositol 4-phosphate 5-kinase (PIP 5-kinase) that generates phosphatidylinositol 4,5-bisphosphate (PI(4,5)P2) which is important for ARF6 dependent endocytosis[51] . Expression of a GTP hydrolysis-resistant ARF6 mutant or overexpression of PIP 5-kinase alpha induces the formation of PI(4,5)P2-positive actin-coated vacuoles that are unable to recycle membrane back to the plasma membrane[51] . These vesicles have been shown to contain ARF6-dependent cargo that remains trapped as they are unable to recruit early endosome markers RAB5 and EEA1 to recycle back[52]. To further test our hypothesis that loss of C-terminal PSD3 phosphorylation leads to aberrant ARF6 activation, we determined if levels of PI(4,5)P2 and recruitment of RAB5 to internalized membrane would be altered in cells expressing S476A mutant. We expressed WT or S476A phosphomutant PSD3 in HEK293T cells along with the PI(4,5)P2 sensor GFP-C1-PLCdelta-PH[51] and endosomal marker BFP-tagged RAB5. In cells expressing WT-PSD3, PI(4,5)P2 was normally localized to the cell membrane, however, cells expressing phosphomutant PSD3 developed numerous large internal vacuoles that were positive for PSD3 and PI(4,5)P2 but devoid of early endosome marker RAB5 (Fig.6c). Total area of internalized vesicles positive for PI(4,5)P2 increased from 4.7% in WT-PSD3 expressing cells to 25.8% in cells expressing the S476A mutant PSD3 (n=23 cells from three experiments, $p<0.0001$) (Fig.6d). Visualization of single z frames images of internalized PIP2 vesicles through super resolution microscopy[53] indicates clear absence of RAB5 on the PSD3 / PI(4,5)P2 positive vesicles (Fig.6e). These data together indicate the phosphorylation of PSD3 at S476 is important for ARF6 mediated endosomal trafficking.

## Discussion

In this study, we utilize a chemical-genetic screen to reveal phosphorylation targets of the autism-associated kinase NUAK1 in the brain. This unbiased approach allowed us to map the

333 basophilic consensus motif preferred by NUAK1. We uncovered direct substrates of NUAK1 in
334 cellular processes NUAK1 has been previously implicated in including splicing, axon growth, and
335 dendrite development, as well as discovered new functions of NUAK1 in regulation of endocytosis
336 and spine maturation (Fig.7a). Among the identified substrates, we focused on the ARF6-specific
337 guanine exchange factor PSD3 and delineated mechanistically how its phosphorylation by
338 NUAK1 negatively controls ARF6-dependent endocytosis and spine maturation (Fig.7b and 7c).
339
340 We report the biochemical characterization of autism-associated NUAK1 variants and show
341 that NUAK1 mutations have differential impact on catalytic activity and subcellular localization.
342 The residue Q161 in the αE-helix in the C-lobe is under high evolutionary constraint and makes
343 key contacts with residues N191 and I192 in the β8 strand that stabilize the catalytic loop of
344 NUAK1. We found that the autism variant Q161E led to a significant decrease in the catalytic
345 activity of NUAK1. The corresponding Q residue in protein kinase A (PKA) is Q149 which has
346 been shown to allosterically regulate the DFG loop during transitions between catalytic active and
347 inactive states[54,55]. The premature termination variant Q433* is predicted to escape nonsense
348 mediated decay, and our data shows that it has intact catalytic activity. However, on expression
349 in neurons and dividing cells, we found that the truncated NUAK1 Q433* is trapped in nuclear
350 speckles positive for SC35. The third NUAK1 disease variant A653V also does not impact
351 catalytic activity but decreases NUAK1 association with nuclear speckles. Our structural analyses
352 suggests that the residue A653 lies in an amphipathic helix within the C-terminal tail. Mechanisms
353 through which the latter two variants have opposing impact on NUAK1 association with nuclear
354 speckles remains to be determined. Collectively, our data suggest that heterozygous autism-
355 associated mutations in NUAK1 are predicted to either decrease substrate phosphorylation or
356 alter substrate availability by shifting the localization of the active kinase between cytoplasm and
357 nuclear speckles, two distinct locations where NUAK1 likely phosphorylates non-overlapping set
358 of substrates. This is highlighted in our dataset of identified NUAK1 substrates that include both
359 nuclear and cytoplasm enriched proteins.
360
361 To shortlist the putative substrate candidates identified in our chemical-genetic screen, we
362 used the following criteria. We reasoned that a true NUAK1 substrate would: (1) be
363 phosphorylated by NUAK1 *in vitro,* (2) show abrogated phosphorylation upon mutation of the
364 identified phospho-site, (3) biochemically interact with the purified kinase, and that (4) purified
365 NUAK1 and substrate in vitro would be sufficient to reconstitute phosphorylation at the identified
366 phosphosite. PSD3, an ARF6 specific GEF, identified in our screen meets all four of the above

367 criteria consistent with a bona fide NUAK1 substrate. PSD3 isoform 3 is phosphorylated at S476
368 (S1001 isoform 1), an evolutionarily conserved site that fits the NUAK1 consensus motif. Notably,
369 mutation of the S476 residue in PSD3 to alanine abolishes all phosphorylation by NUAK1,
370 indicating it is the only site within PSD3 that is phosphorylated by NUAK1. The phosphosite is
371 situated in the C-terminal tail of PSD3 following the PH domain and the coiled coil region which
372 binds cortical actin. The C-terminus of PSD3 mediates its plasma membrane association which
373 is required for activation of ARF6 at the membrane via the catalytic SEC7 domain. While it is
374 unlikely that phosphorylation at S476 directly impacts SEC7 domain mediated GEF activity, it can
375 indirectly increase ARF6 activation by promoting membrane or actin association of PSD3.
376 Accumulation of PI(4,5)P2 positive vesicles that fail to acquire endosomal markers such as RAB5
377 in cells expressing phosphomutant PSD3 are phenotypically similar to expression of ARF6 Q67L
378 mutant which cannot hydrolyze GTP. Another possibility is that phosphorylation of the PSD3 tail
379 does not impact ARF6 activity but regulates recruitment of ARF6 GAPs that convert GTP-bound
380 ARF6 to GDP.
381
382 It is important to note that copy number variation and missense mutations in PSD3 have been
383 identified in patients with autism spectrum disorder[29,30,56]. ARF6 GTPase is an important regulator
384 of actin dynamics and membrane trafficking, and plays an important role in neurite development,
385 axon growth, and synaptic plasticity[57]. PSD3 is enriched within dendritic spines, and our data
386 shows that abolishing NUAK1 mediated phosphorylation at S476 further increases PSD3 spine
387 enrichment, as well as causes loss of filopodial protrusions and stabilization of mature mushroom
388 dendritic spines. This is consistent with the effect of expression of fast cycling ARF6 mutant T157A
389 which increases the conversion of filopodia into mature spines[50]. The impact of PSD3 variants
390 associated with autism spectrum disorder on spine stability and ARF6 activity has not been tested
391 and will be subject of future investigation. In addition to autism, both NUAK1 and PSD3/ARF6
392 have been implicated in cancer progression, fatty liver and metabolic disease[19,58–62]. Our study
393 raises the interesting possibility that NUAK1 mediated phosphorylation of PSD3 underlies diverse
394 physiological effects of ARF6 dependent endocytic trafficking.
395
396 **Acknowledgement**
397 We are grateful for funding support by the National Institutes of Health to SY (R01MH121674,
398 R01MH130336), JS (T32 GM007750) and SEO (R01GM129090, R21CA288806). Funding for
399 the purchase of ELYRA7 Lattice SIM microscope was generously provided by the Murdock
400 Foundation Equipment Grant to SY with matching funds from the University of Washington. This

study used an EASY-nLC1200 UHPLC and Thermo Scientific Orbitrap Fusion Lumos Tribrid mass spectrometer purchased with funding from a National Institutes of Health SIG grant S10OD021502.

**Author Contributions**

J.S. designed and performed all experiments under the supervision of S.Y. D.M. ran the proteomics samples on the LC-MS/MS and performed data analysis under the supervision of S.E.O. A.S. performed dendritic spine morphology and vesicle area quantifications. M.C. performed Alphafold predictions and Pymol modeling. Manuscript was written by J.S. and S.Y., and edited by all authors.

**Methods**

**Expression Constructs, Cloning and Reagents**

Full-length human NUAK1 was PCR amplified from K84M kinase-DEAD Nuak1-3x Flag (Addgene #97219) and inserted into vector sfGFP-C1 (Addgene #54579) or PRK5-HA (PMID: 28065648) using PCR amplification followed by Gibson Assembly (NEB). The K84M mutation was corrected using primers to generate WT NUAK1. All mutants of NUAK1 (K84M, M132A, M132G, Q161E, Q433*, A653V) were generated using PCR amplification followed by Gibson assembly (NEB). NUAK1 Q433* was cloned into the bacterial expression vector 8xHis-MsyB (HM) (Addgene #112570) to generate HM-NUAK1 1-433 using PCR amplification followed by Gibson assembly (NEB). The K84M or M132G mutations were introduced in this plasmid using PCR amplification followed by Gibson assembly (NEB). Full-length human PSD3 isoform 1 (canonical) was obtained from DNASU and inserted into an N-terminal V5 mammalian expression using Gateway cloning (Thermo). PSD3 isoform 3, which is 513 amino acids long, shares all except the first 11 amino acids with isoform 1. PSD3 isoform 3 was cloned using PCR amplification to insert the 11 amino acids at the N-terminus, followed by Gibson assembly (NEB). PSD3-isoform 3 E114K and S476A point mutations were cloning using PCR amplification followed by Gibson assembly (NEB). V5-PSD3-iso3-sfGFP was cloned by inserting sfGFP from sfGFP-C1 vector (Addgene #54579) at the C-terminus of PSD3 followed by a stop codon using PCR amplification and Gibson Assembly. mCherry-V5-PSD3-iso3 was cloned by inserting the mCherry from mCherry-Rab5 (Addgene #49201) upstream of V5-PSD3-iso3 using PCR amplification followed by Gibson Assembly (NEB). GST-PSD3-coiled coil tail was generated by PCR amplification of amino acids 378-513 of PSD3-isoform 3 followed by Gibson Assembly (NEB) with PCR-amplified pGex-4T3 vector (Addgene #31669).

435 Arf6-mNeonGreen was obtained from Addgene, and the mNeonGreen was exchanged for
436 mScarlet from mScarlet-Rab7 (Addgene #169068) using PCR amplification and Gibson Assembly
437 (NEB). Arf6-mScarlet T44N (DN) mutation was introduced using PCR amplification followed by
438 Gibson Assembly (NEB).

| Construct name | Source |
|---|---|
| Myristoyl-tdtomato | Yadav et al, *Neuron*, 2017 (PMID 28065648) |
| PRK5-HA vector | Yadav et al, *Neuron*, 2017 (PMID 28065648) |
| Rab5b-BFP | Addgene #49147 |
| Arf6-mNeonGreen WT | Addgene #162027 |
| Arf6-mScarlet (WT, T44N) | Cloned in this study |
| PSD3 in pDONR221 | DNASU #HsCD00296934 |
| GFP-C1-PLC-delta-PH | Addgene # 21179 |
| K84M kinase-DEAD Nuak1-3x Flag | Addgene #97219 |
| pExp-MsyB | Addgene #112570 |
| GST-PSD3-CC-tail | Cloned in this study |
| PRK5-HA-NUAK1 (WT, K84M, M132G, M132A) | Cloned in this study |
| sfGFP-C1-NUAK1 (WT, K84M, Q161E, Q433*, A653V) | Cloned in this study |
| pGEX-PPP1R12A wt | Addgene #31669 |
| His-MsyB-NUAK1 1-433 (WT, K84M, M132G) | Cloned in this study |
| sfGFP-C1 | Addgene # 54579 |

439

440 **Cell Line Maintenance and Transfection**

441 HEK293T cells were grown in Dulbecco's modified Eagle's medium (Thermo Fisher
442 Scientific, Gibco) with 10% fetal bovine serum (Axenia BioLogix) and 1% penicillin-streptomycin
443 (Invitrogen). Cells were maintained at 5% $CO_2$ and 37°C and passaged every 3 to 4 days. Cells
444 were tested for mycoplasma using the Abm PCR-based kit. For biochemical experiments,
445 HEK293T cells were transfected with 0.5-1 ug plasmid DNA using the JetOptimus system
446 (Genesee Scientific) following the manufacturer's instructions. For confocal imaging, HEK293T
447 cells were transfected with 100-500 ng plasmid DNA using Lipofectamine 2000 and Optimem
448 (Thermo Scientific) according to the manufacturer's instructions.

449 Primary neurons were obtained from dissociating hippocampi obtained from embryonic
450 day 18 (E18) Sprague-Dawley rat (Envigo). Animal work was performed under University of

451 Washington Institutional Animal Care and Use Committee approved protocol 4421-01. Rat
452 embryos were trypsin-dissociated and plated at a density of 150,000 neurons per 18-mm glass
453 coverslip (Thermo Fisher Scientific) or 450,000 neurons per 35-mm glass-bottom dish (MaTek),
454 which were coated with poly-D-lysine (0.06 mg/ml; Sigma-Aldrich) and laminin (0.0025 mg/ml;
455 Sigma-Aldrich). Plating medium containing heat-inactivated 10% fetal bovine serum (HyClone),
456 0.45% dextrose, sodium pyruvate (0.11 mg/ml), and 2 mM glutamine in minimum essential
457 medium with Earle's Balanced Salt Solution was used. Medium was changed 4 hours after
458 seeding neurons into maintenance medium consisting of Neurobasal medium (Invitrogen), 2%
459 B27 (Invitrogen), penicillin (50 U/ml) and streptomycin (50 µg/ml), and 0.5 mM Glutamax
460 (Thermo). Half of the medium was replaced with new maintenance medium every 3 to 4 days.
461 For exogenous gene expression, neurons were transfected with 0.5 to 1.0 µg of plasmid DNA per
462 coverslip in a 12-well plate (or 1 to 2 µg of DNA per 35-mm dish) using Lipofectamine 2000
463 (Invitrogen) following the manufacturer's guide.
464 WTC11 iPSCs (Corielle) were differentiated into neuroprogenitor cells (NPCs) as reported
465 previously[63] . Stem cells were treated with 1U/mL Dispase, lifted using a cell scraper,
466 resuspended in mTeSR media (STEMCELL Technologies) containing 10µm ROCK Inhibitor
467 (Selleck Chemical), and then transferred to uncoated T25 flasks for embryoid body (EB)
468 formation. After 24–48 hours (Day 0), EBs were gravity settled and transferred to new uncoated
469 T25 flasks in neural media (DMEM/F12 (Gibco), 1% N-2 supplement (Gibco), 1% Non-essential
470 amino acids (Gibco), 2µg/mL Heparin, 1% Penicillin/Streptomycin [Gibco]) containing small
471 molecule TGF-β/SMAD inhibitors, SB431542 (5µM; Peprotech) and LDN193189 (0.25µM;
472 Peprotech). On Day 3, EBs were transferred to Matrigel (1:50 dilution; Corning)-coated 6 well
473 plates in fresh neural media with SB and LDN. Media was changed with neural media without SB
474 and LDN every other day or as needed until Day 11 for formation of neural rosettes. On Day 11,
475 neuroepithelia were mechanically lifted using a cell scraper and transferred to uncoated T25
476 flasks in neural media. Neurospheres were fed with neural media every other day, or as needed,
477 until Day 25. On Day 25, neurospheres were plated onto Matrigel-coated plates in STEMDiff™
478 Neural Progenitor Media (STEMCELL Technologies) and NPCs were obtained. NPCs were tested
479 for neural progenitor markers Nestin (Invitrogen) and PAX6 (Sigma).
480
481 **Protein Purification**
482 *HM-NUAK1 purification*
483 NUAK1 (WT, KD, or M132G) were inserted into 8x-His-tagged pExp-MsyB (HM) vector for
484 bacterial expression and purification. Due to poor expression of full-length NUAK1 1-661, we

485 elected to use NUAK1 1-433, which is kinase active but contains less unstructured domains than
486 full-length NUAK1. Expression of NUAK1 1-433 was dramatically improved over full length, so we
487 moved forward with purification of HM-NUAK1 1-433 WT, K84M, and M132G. HM-NUAK1 1-433
488 WT, K84M, or M132G were transformed into BL21 *E. coli* and sequenced using full-plasmid
489 sequencing (Plasmidsaurus) to confirm the sequences were correct. 50 mL cultures of HM-
490 NUAK1 were grown overnight with Carb and used to inoculate 1L cultures, which were grown at
491 37C with 220 rpm shaking until Optical Density (OD) of 0.6-0.8 was reached. At this point, the
492 incubator was cooled to 20C (room temperature), and IPTG was added to all cultures for a final
493 concentration of 0.4mM. Protein induction was performed overnight at 20C with 220 rpm shaking.
494 Bacteria were pelleted the next day by spinning at 3,200 rcf at 4C for 15 minutes, followed by
495 removal of LB and addition of 30 mL 1x DPBS. The cultures suspended in PBS were transferred
496 to 50 mL conical tubes and spun at 3,200g at 4C for 15 minutes. The PBS was then removed,
497 and 25 mL lysis buffer (20 mM Tris pH 7.5, 200 mM NaCl, 0.4 mM TCEP, 20 mM imidazole, 1x
498 cOmplete protease inhibitor (Sigma), 0.1% PMSF, and 10% glycerol) was added to the tube.
499 Bacteria were lysed using sonication at 25% power for 3.5 minutes, followed by centrifugation at
500 24,500g for 60 minutes at 4C to pellet debris. Following centrifugation, the supernatant was added
501 to 1 mL HisPur Ni-NTA resin (Thermo) for 60 min at 4C with rotation to bind HM-NUAK1 to the
502 beads. After binding, beads were added to a fritted column and the supernatant allowed to drain
503 by gravity. The beads were then washed with 20 mL lysis buffer, followed by the addition of lysis
504 buffer + 200 mM imidazole. This high imidazole buffer was incubated with the beads for 5 minutes,
505 after which eluted protein was collected every 10 minutes for a total of 6 elutions, and quantified
506 using Pierce 600nm protein assay (Thermo). The eluted protein was then incubated with
507 sulphopropyl (SP) beads (GE healthcare) to enrich for acidic proteins for 1 hour rotating at 4C,
508 followed by elution with 450mM NaCl. Finally, proteins were concentrated to a final concentration
509 of ~10 ug/mL using concentrators with a 30kD molecular weight cutoff (Thermo). Following
510 concentration, protein aliquots were flash frozen in liquid nitrogen and stored at -80C. All
511 purification samples were assayed for purity by SDS-Page, Coomassie staining, and Western
512 blotting with anti-His-HRP antibody (Proteintech).

513 *GST-PSD3 purification*

514 PSD3-CC tail (WT or S>A) was cloned into the pGEX-4T3 bacterial expression vector,
515 transformed into BL21 *E. coli*, and sequenced using full-plasmid sequencing (Plasmidsaurus). 25
516 mL overnight cultures of GST-PSD3 were grown overnight with Carb and used to inoculate 1L
517 cultures, which were grown at 37C with 220 rpm shaking until Optical Density (OD) of 0.6-0.8 was
518 reached. At this point, the incubator was cooled to 30C, and IPTG was added to all cultures for a

519 final concentration of 0.3mM. Protein induction was performed for 2 hours at 30C with 220 rpm
520 shaking. Bacteria were pelleted by spinning at 3,200 rcf at 4C for 15 minutes, followed by removal
521 of LB and addition of 30 mL 1x DPBS. The cultures suspended in PBS were transferred to 50 mL
522 conical tubes and spun at 3,200g at 4C for 15 minutes. The PBS was then removed, and samples
523 were resuspended in 7 mL lysis buffer (50mM Tris pH 8.0, 200mM NaCl, 5mM EDTA, 10%
524 glycerol, 5mM DTT, 1x cOmplete protease inhibitor (Sigma), 0.1% PMSF). 4 mg of lysozyme was
525 added to each sample, followed by incubation for 30 minutes on ice with occasional mixing. After
526 this step, Triton was added to the sample for a final concentration of 1%, followed by lysis with
527 sonication as described above. After lysis, samples were centrifuged at 24,500g for 60 minutes
528 at 4C to pellet debris. Columns for batch binding were prepared using 500 uL of glutathione resin
529 (Thermo) and 10 mL binding buffer (50mM Tris pH 8.0, 200mM KCl, 1mM DTT). The buffer was
530 removed prior to the addition of the post-centrifugation bacterial supernatant to the beads. The
531 binding of GST-PSD3 to the beads was performed overnight at 4C with rotation. The next day,
532 columns were washed 2x with 15 mL wash buffer (50mM Tris pH 8.0, 200mM KCl, 0.1% Tween-
533 20 1mM DTT), followed by 2x washes with 1 mL binding buffer to remove detergent. Samples
534 were then eluted in binding buffer + 25 mM glutathione in 500 uL fractions every 10 minutes, for
535 a total of 6 elutions. Protein concentration was quantified using Pierce 600nm protein assay
536 (Thermo), and purification samples were assayed for purity by SDS-Page, Coomassie staining,
537 and Western blotting with anti-GST-HRP antibody (Thermo). Following protein quantification,
538 GST-PSD3 was diluted to 1 mg/mL final concentration with binding buffer, and aliquots were flash
539 frozen in liquid nitrogen and stored at -80C.
540
541 **Immunoprecipitation and Kinase Assay**
542 HEK293T cells were transfected with 0.5-1 ug plasmid DNA using the JetOptimus system
543 according to the manufacturer's instructions (Genesee Scientific). After overnight transfections,
544 cells were lysed in HKT lysis buffer (25 mM HEPES pH 7.2, 150 mM KCl, 1% Triton X-100, 1mM
545 DTT) with 1x cOmplete protease inhibitor (Sigma). Lysate was then spun for 10 minutes at
546 15,000g at 4C to pellet out cell debris. For pre-conjugated beads (HA, V5), beads were
547 equilibrated with 2x HKT washes, followed by addition of 1 mL cell lysate for 30 uL equilibrated
548 beads. For non-conjugated beads (Protein G), beads were equilibrated with 2x HKT washes,
549 followed by pre-clearing of 1 mL cell lysate with 15 uL equilibrated beads for 30-60 min at 4C
550 rotating. 1 ug of mouse primary antibody (anti-GFP, Roche) was conjugated to 30 uL of Protein
551 G beads during this pre-clear step, followed by addition of pre-cleared lysate to the conjugated
552 beads for immunoprecipitation. Proteins were immunoprecipitated for 3-16 hours at 4C with

553 rotation. Following IP, samples were washed 2x with HKT, 1x with high salt HKT (25 mM HEPES
554 pH 7.2, 1 M NaCl, 1% Triton X-100, 1mM DTT) for 10 minutes, 2x with HK buffer (25 mM HEPES
555 pH 7.2, 1 M NaCl, 1mM DTT), and 2x with kinase buffer (20 mM Tris HCl pH 7.5, 10 mM MgCl2,
556 1 mM DTT, 1x cOmplete protease inhibitor). Following bead washes, kinase labeling reaction was
557 performed for 45 minutes at 30C on a shaking heat block (Thermo) in kinase buffer with 0.5mM
558 ATP (Sigma) or ATPɣS (Thermo) and 2x Halt Phosphatase inhibitor (Thermo). Following the
559 kinase reaction, samples with normal ATP were quenched by the addition of 4X Lammeli-SDS
560 sample buffer (Thermo) with 200mM DTT. Labeling was quenched in samples with ATPgS by the
561 addition of EDTA to a final of concentration of 50mM, and thiophosphates were then alkylated
562 with p-nitrobenzyl mesylate (pNBM, Sigma) at a final concentration of 6.67mM for 45 minutes at
563 room temperature. After alkylation of the ATPgS-containing samples, the reaction was quenched
564 by the addition of 4X Lammeli-SDS sample buffer (Thermo) with 200mM DTT. For co-IP
565 experiments, 0.5μg of V5-PSD3 was co-transfected with 0.5μg of HA-NUAK1 WT or HA-empty
566 vector with JetOptimus (Genesee Scientific) as above. This was followed by lysis, equilibration of
567 beads, and immunoprecipitation with either HA or V5-conjugated beads for 3 hours. Following IP,
568 samples were washed 3x with HKT and 3x with HK, followed by addition of 4X Lammeli-SDS
569 sample buffer (Thermo) with 200mM DTT.
570
571 **Antibodies and Reagents**

| Antibody/Reagent | Company | Catalog number |
|---|---|---|
| HA beads | Sigma | E6779-1ML |
| V5 beads | Sigma | A7345-1ML |
| HisPur Ni-NTA beads | ThermoFisher | 88221 |
| Glutathione beads | ThermoFisher | 16100 |
| Pierce Protein G beads | ThermoFisher | 20398 |
| Anti-NUAK1 | MRC PPU | Sheep 628B |
| Anti-GFP (Roche) | Sigma | 11814460001 |
| Anti-p-S/T | Phosphosolutions | PP2551 |
| Anti-pTE | Abcam | ab92570 |
| Anti-HA | Proteintech | 66006-2-Ig |
| His-HRP | Proteintech | HRP-66005 |
| GST-HRP | ThermoFisher | MA4-004-HRP |
| Anti-V5 | ThermoFisher | R960-25 |

| | | |
|---|---|---|
| Anti-MAP2 | Abcam | ab5392 |
| Phenyl-ATPɣS | Axxora | BLG-P044 |
| Furfuryl-ATPɣS | Axxora | BLG-F008-05 |
| Benzyl-ATPɣS | Axxora | BLG-B072 |
| ATPɣS | Thermo | 40-801-0 |
| pNBM | Sigma | SML3810-25MG |

572

573 **Confocal Microscopy**

574 Live and fixed cell confocal imaging was performed on a Nikon Ti2 Eclipse-CSU-X1 confocal
575 spinning disk microscope equipped with four laser lines—405, 488, 561, and 670 nm—and the
576 Nikon Elements software. An Andor Zyla4.2 Plus sCMOS camera was used for image acquisition.
577 The microscope was caged within the OkoLab environmental control setup, enabling temperature
578 and $CO_2$ control during live imaging. Imaging was performed using Nikon 1.49 100×, Apo 60×, or
579 40× oil objectives. All image analyses were done using the open access Fiji software.

580

581 **Super Resolution Microscopy**

582 The Zeiss ELYRA7 Lattice SIM2 structural illumination microscope was used for super resolution
583 imaging. Live cell imaging was performed on a Zeiss Axio Observer 7 - Lattice SIM inverted
584 microscope for super resolution microscopy equipped with four laser lines – 405 nm (50mW), 488
585 nm (100mW), 561 nm (100mW) and 642 nm (150mW) – and the ZEN imaging software. Two
586 Hamamatsu ORCA-Fusion BT sCMOS cameras were used for simultaneous image acquisition.
587 The microscope was equipped with a Zeiss Stage Top incubation and gas system for Lattice SIM
588 inverted microscopes, enabling temperature, humidity, and CO2 control during live imaging.
589 Imaging was performed using Plan-Apochromat 63x/1.40 oil DIC objective.

590

591 **Immunofluorescence and Western Blotting**

592 All cells, including neurons, were fixed using warm 4% paraformaldehyde with 4% sucrose for
593 20 min at room temperature followed by three washes with 1x phosphate-buffered saline (PBS).
594 One-hour incubation with blocking buffer [4% normal donkey serum, 0.2 M glycine (pH 7.4), and
595 0.1% Triton X-100, in 1x PBS] was followed by overnight incubation with primary antibody at
596 1:100-1000 dilution in blocking buffer at 4°C. After six 5-min washes in PBS, cells were incubated
597 with secondary antibody at 1:1000 dilution in blocking buffer for overnight at 4°C. Coverslips were
598 washed 6 times in PBS and then mounted onto microscope glass slides with Fluoromount-G
599 (EMS) and sealed with clear nail polish (EMS).

600 Samples for Western blot analysis were treated with NuPAGE LDS sample buffer (4×)
601 (Invitrogen) with Dithiothreitol (DTT) at 200mM and subsequently heated for 10 min at 95°C.
602 Samples were electrophoresed on NuPAGE 4 to 12% Bis-Tris polyacrylamide gels (Invitrogen)
603 with NuPAGE MOPS or MES running buffer (Invitrogen). Western blots were transferred to
604 polyvinylidene difluoride membrane Immobilon-P (MilliporeSigma) with transfer buffer [25 mM
605 Tris, 192 mM glycine, 0.1% SDS and 20% (v/v) methanol]. Transferred blots were blocked in 5%
606 nonfat dry milk or 5% Bovine Serum Album (Equitech Bio) and subjected to primary antibody
607 overnight, washed 3x with blocking buffer, and incubated 3 hours at room temperature with
608 horseradish peroxidase–conjugated secondary antibody before visualization with Pierce
609 SuperSignal West Pico PLUS Chemiluminescent Substrate (Thermo Fisher Scientific). Western
610 blot images were obtained using the ChemiDoc Imaging System (Bio-Rad). Western blot images
611 were analyzed and quantified using Image Lab Software for Mac Version 6.1 (Bio-Rad).
612
613 **Mouse Brain Lysate**
614 To prepare mouse brain lysate, P13-P15 C57BL/6 mice pups of both sexes were euthanized by
615 CO2 (5psi for 10min) followed by decapitation. The brains were dissected out and incubated in
616 high detergent lysis buffer (20mM Tris pH7.5, 100mM NaCl, 10mM MgCl2, 0.5mM DTT, 1%
617 TritonX-100, 1% deoxycholic acid, and 1x cOmplete protease inhibitor) on ice for 30min.
618 Homogenization was achieved by sonication. Supernatant was collected after centrifugation at
619 14,000g at 4°C for 10 min, aliquots were prepared by diluting with lysis buffer without detergent
620 to 20μg/μl, flash frozen in liquid nitrogen and stored at -80°C.
621
622 **NUAK1 Substrate Labeling and Covalent Capture**
623 Covalent capture to identify NUAK1 kinase substrates using mass spectrometry was done as
624 previously described[14,15,22,23]. Briefly, HA-tagged NUAK1 M132G was purified from HEK293T cells
625 by affinity purification using HA antibody-coated beads. Cells expressing HA-tagged kinase-dead
626 NUAK1-K84M were used as negative controls. Cells were lysed with 25mM HEPES pH 7.2,
627 150mM KCl, 1x cOmplete protease inhibitor cocktail (Sigma), 1x Halt phosphatase inhibitor
628 (Thermo), 1 mM DTT, 1 mM EDTA, and 1% Triton X-100. Lysate was incubated on ice for 30 min
629 with frequent vortexing to lyse cells, followed by centrifugation at 20,000g for 15 min. Supernatant
630 was incubated with 30μL anti-HA resin for 3hr rotating at 4C. 100μl brain lysate at 20μg/μl protein
631 concentration was used for labeling by NUAK1-AS or NUAK1-KD. A total of 5 experimental
632 replicates each for NUAK1-AS or NUAK1-KD were completed with p15 mouse brain lysate.

633 The labeling reaction comprised of 1μM cAMP-dependent protein kinase inhibitor (PKI 5-24,
634 Tocris), 0.2μM protein kinase C inhibitor (Bisindolylmaleimide-I, Calbiochem), 3mM GTP (Sigma),
635 100μM ATP (Sigma), 1μM okadaic acid (Sigma), 2x Halt Phosphatase inhibitor (ThermoFisher)
636 and 0.5mM Furfuryl-ATP-γ-S (Axxora).
637 Labeling of the brain lysate was quenched by addition of EDTA to 50mM final concentration. The
638 labeled reaction was denatured by adding solid urea (60% w/v) and TCEP (10mM final
639 concentration) and incubating at 55°C for an hour. Samples were then diluted with two volumes
640 of ammonium bicarbonate (Sigma) and two volumes of TCEP (to maintain 10 mM final
641 concentration) and the pH adjusted to 8.0, then digested with Trypsin (Promega, sequencing
642 grade #V5113) with overnight rotation at 37C. Trypsin was quenched the following day by adding
643 0.5% TFA (Trifluoroacetic acid, Sigma).
644 Peptides were ascertained to be at pH 3.0, then desalted and cleaned using C18 cartridges
645 (Waters Sep-Pak Classic C18 Cartridges), and finally eluted by 70% Acetonitrile (ACN) and 0.1%
646 TFA. Peptide solution was reduced in volume by SpeedVac and final solution adjusted to 50%
647 ACN and 50mM HEPES pH 7.3.
648 Samples were evenly adjusted to pH7.0 using 5% NaOH, incubated with SulfoLink Coupling
649 Resin (ThermoFisher, 20401) and mixed overnight on a nutator at room temperature protected
650 from light. Addition of 25μg Bovine Serum Albumin (BSA) to the beads prior to sample addition
651 ensured low background binding. The following day, the beads were washed over equilibrated
652 fritted columns (Sigma) sequentially using Ultrapure H2O (Thermo), 5M NaCl, 50% ACN, 5%
653 Formic Acid and 1mM DTT. Bound thio-phospho-peptides were eluted through hydrolysis reaction
654 by addition of Oxone (1mg/ml Oxone in ddH2O freshly prepared, Sigma 228036). The resulting
655 phosphopeptides were extracted and desalted using C18 StageTips according to the published
656 protocol[24].
657
658 **Reversed-Phase LC-MS/MS Analysis**
659 Peptide samples were separated on an EASY-nLC 1200 System (Thermo Fisher Scientific) using
660 20 cm long fused silica capillary columns (100 μm ID, laser pulled in-house with Sutter P-2000,
661 Novato CA) packed with 3 μm 120 Å reversed phase C18 beads (Dr. Maisch, Ammerbuch,
662 DE). The LC gradient was 90 min long with 5–35% B at 300 nL/min. LC solvent A was 0.5% (v/v)
663 aq. acetic acid and LC solvent B was 80% acetonitrile in 0.5% (v/v) acetic acid. MS data was
664 collected with a Thermo Fisher Scientific Orbitrap Fusion Lumos using a data-independent
665 acquisition (DIA) method with a 120K resolution Orbitrap MS1 scan and 12 m/z isolation window,
666 30K resolution Orbitrap HCD MS2 scans for precursors from 400-1000 m/z.

667

668 **Protein and Phosphosite Identification**

669 Data .raw files were converted to .mzML using MSConvert 3.0.24285 and searched using
670 FragPipe version 21.1 and MSFragger version 4.0, with quantification through DIA-NN version
671 1.8.2[64,65]. The database search was against the UniProt mouse protein sequence database
672 (downloaded 02-14-2024) with supplemental spike-in of common contaminants, containing 17642
673 sequences and 17642 reverse-sequence decoys, as well as the sequence for human NUAK1.
674 For the MSFragger analysis, both precursor and initial fragment mass tolerances were set to
675 20 ppm. Enzyme specificity was set to "strictrypsin" and up to two missed cleavages were
676 allowed. Oxidized Met, acetylated N-termini, and phosphorylated Ser/Thr/Tyr were set as variable
677 modifications and carbamidomethylated Cys was a fixed modification. The maximum number of
678 variable modifications per peptide was set to 3. FragPipe/DIA-NN output files were processed
679 using a Python script to extract +/- 7 AA sequence flanking identified phosphosites from the
680 FASTA file.

681

682 **Database Usage**

683 Developing and adult human brain transcriptomics data were obtained and plotted using HBT
684 database (https://hbatlas.org/). These data were generated using Affymetrix GeneChip Human
685 Exon 1.0 ST Arrays from over 1340 tissue samples sampled from both hemispheres of
686 postmortem human brains, with specimens ranging from embryonic development to adulthood
687 and representative of both males and females from multiple ethnicities. Allen Brain Atlas was used
688 to search for NUAK1 mRNA expression in the mouse brain (https://mouse.brain-
689 map.org/experiment/show/73497621) as well as PSD3 mRNA expression (https://mouse.brain-
690 map.org/experiment/show/69095967). Evolutionary conservation analysis for both NUAK1 and
691 PSD3 was performed using the ConSurf-DB web server[32]. Amphipathic helix prediction was
692 performed using the NUAK1 protein sequence from Uniprot and the Heliquest[35]. NUAK1
693 consensus sequence and phosphorylation preference for substrates was determined using the
694 publicly available Kinase Library database which was generated using the data from Johnson et
695 al, 2023[42].

696

697 **Molecular Modeling of NUAK1 and its Substrates**

698 Prediction of NUAK1(O60285) with PSD3(Q9NYI0) and NUAK1(O60285) with PP1beta(P62140)
699 and MYPT1(O14974) was obtained using Alphafold3[33]. Alphafold3 was installed via GitHub
700 (https://github.com/google-deepmind/alphafold3) on a machine running Ubuntu 24.04 LTS with

701 two Nvidia A6000 48GB GPUs. Structural figures were prepared in PyMOL (Schrodinger).
702 Predictions were performed with 20 recycles with 5 diffusion samples per seed. Multiple seeds
703 (217, 275, 428, 551, and 924) were used for random number generation to increase robustness
704 of prediction.
705
706 **Statistics and Reproducibility**
707 Statistical analyses were performed with GraphPad Prism (version 10.0). No statistical
708 method was used to pre- determine sample size, and no data were excluded from the analyses.
709 The experiments were not randomized and investigators were not blinded during experiments
710 and data analysis. All experiments were performed in at least three independent replicates.
711
712

713 **References**

714


715 1. Manning, G., Whyte, D. B., Martinez, R., Hunter, T. & Sudarsanam, S. The protein kinase complement
716 of the human genome. *Science* **298**, 1912–1934 (2002).

717 2. Courchet, V. *et al.* Haploinsufficiency of autism spectrum disorder candidate gene NUAK1 impairs
718 cortical development and behavior in mice. *Nat. Commun.* **9**, 4289 (2018).

719 3. Bennison, S. A., Liu, X. & Toyo-oka, K. Nuak kinase signaling in development and disease of the
720 central nervous system. *Cell. Signal.* **100**, 110472 (2022).

721 4. Ferrarelli, L. K. A tauopathy kinase. *Sci. Signal.* **9**, (2016).

722 5. Lasagna-Reeves, C. A. *et al.* Reduction of Nuak1 Decreases Tau and Reverses Phenotypes in a
723 Tauopathy Mouse Model. *Neuron* **92**, 407–418 (2016).

724 6. Taylor, L. W. *et al.* p-tau Ser356 is associated with Alzheimer's disease pathology and is lowered in
725 brain slice cultures using the NUAK inhibitor WZ4003. *Acta Neuropathol.* **147**, 7 (2024).

726 7. Zhang, T. *et al.* NUAK1 promotes organ fibrosis via YAP and TGF-β/SMAD signaling. *Sci. Transl.*
727 *Med.* **14**, eaaz4028 (2022).

728 8. Carney, E. F. NUAK1 promotes kidney fibrosis. *Nat. Rev. Nephrol.* **18**, 345–345 (2022).

729 9. Ni, X., Pan, F., Lang, Y. K. & Zhang, W. Prognostic significance of NUAK1 and its association with
730 immune infiltration in stomach adenocarcinoma. *Discov. Oncol.* **15**, (2024).

731 10. Golkowski, M. *et al.* Pharmacoproteomics Identifies Kinase Pathways that Drive the Epithelial-
732 Mesenchymal Transition and Drug Resistance in Hepatocellular Carcinoma. *Cell Syst* **11**, 196-207.e7
733 (2020).

734 11. Yao, C.-Y. *et al.* NUAK1 acts as a novel regulator of PD-L1 via activating GSK-3β/β-catenin
735 pathway in hepatocellular carcinoma. *Mol. Med.* **31**, 38 (2025).

736 12. Whyte, D. *et al.* NUAK1 governs centrosome replication in pancreatic cancer via MYPT1/PP1β and
737 GSK3β-dependent regulation of PLK4. *Mol. Oncol.* **17**, 1212–1227 (2023).

738 13. Inazuka, F. *et al.* Muscle-specific knock-out of NUAK family SNF1-like kinase 1 (NUAK1) prevents
739 high fat diet-induced glucose intolerance. *J. Biol. Chem.* **287**, 16379–89 (2012).

740 14. Crunkhorn, S. NUAK1 inhibition prevents fibrosis. *Nat. Rev. Drug Discov.* **21**, 338–338 (2022).

741 15. Courchet, J. *et al.* Terminal Axon Branching Is Regulated by the LKB1-NUAK1 Kinase Pathway via
742 Presynaptic Mitochondrial Capture. *Cell* **153**, 1510–1525 (2013).

743 16. Lanfranchi, M. *et al.* The AMPK-related kinase NUAK1 controls cortical axons branching by locally
744 modulating mitochondrial metabolic functions. *Nat. Commun.* **15**, 2487 (2024).

745 17. Zagórska, A. *et al.* New Roles for the LKB1-NUAK Pathway in Controlling Myosin Phosphatase
746 Complexes and Cell Adhesion. *Sci Signal* **3**, ra25 (2010).

747 18. Hou, X. *et al.* A new role of NUAK1: directly phosphorylating p53 and regulating cell proliferation.
748 *Oncogene* **30**, 2933–2942 (2011).

749 19. Cullen, N. M. *et al.* NUAK kinases: Signaling mechanisms and therapeutic applications. *J. Biol.*
750 *Chem.* **301**, 110565 (2025).

751 20. Lizcano, J. M. *et al.* LKB1 is a master kinase that activates 13 kinases of the AMPK subfamily,
752 including MARK/PAR-1. *EMBO J.* **23**, 833–843 (2004).

753 21. Suzuki, A., Ogura, T. & Esumi, H. NDR2 Acts as the Upstream Kinase of ARK5 during Insulin-like
754 Growth Factor-1 Signaling*. *J. Biol. Chem.* **281**, 13915–13921 (2006).

755 22. Suzuki, A. *et al.* Identification of a Novel Protein Kinase Mediating Akt Survival Signaling to the
756 ATM Protein*. *J. Biol. Chem.* **278**, 48–53 (2003).

757 23. Monteverde, T. *et al.* Calcium signalling links MYC to NUAK1. *Oncogene* **37**, 982–992 (2018).

758 24. Cossa, G. *et al.* Localized Inhibition of Protein Phosphatase 1 by NUAK1 Promotes Spliceosome
759 Activity and Reveals a MYC-Sensitive Feedback Control of Transcription. *Mol. Cell* **77**, 1322-1339.e11
760 (2020).

761 25. Palma, M. *et al.* Identification of a nuclear localization signal and importin beta members mediating
762 NUAK1 nuclear import inhibited by oxidative stress. *J. Cell. Biochem.* **120**, 16088–16107 (2019).

763 26. Blazejewski, S. M., Bennison, S. A., Liu, X. & Toyo-oka, K. High-throughput kinase inhibitor
764 screening reveals roles for Aurora and Nuak kinases in neurite initiation and dendritic branching. *Sci.*
765 *Rep.* **11**, 8156 (2021).

766 27. Satoh, D. & Arber, S. Carving Axon Arbors to Fit: Master Directs One Kinase at a Time. *Cell* **153**,
767 1425–1426 (2013).

768 28. Kang, H. J. *et al.* Spatio-temporal transcriptome of the human brain. *Nature* **478**, 483–489 (2011).

769 29. Iossifov, I. *et al.* De Novo Gene Disruptions in Children on the Autistic Spectrum. *Neuron* **74**, 285–
770 299 (2012).

771 30. Iossifov, I. *et al.* The contribution of de novo coding mutations to autism spectrum disorder. *Nature*
772 **515**, 216–221 (2014).

773 31. Wang, T. *et al.* De novo genic mutations among a Chinese autism spectrum disorder cohort. *Nat.*
774 *Commun.* **7**, 13316 (2016).

775 32. Chorin, A. B. *et al.* ConSurf-DB: An accessible repository for the evolutionary conservation patterns
776 of the majority of PDB proteins. *Protein Sci.* **29**, 258–267 (2020).

777 33. Abramson, J. *et al.* Accurate structure prediction of biomolecular interactions with AlphaFold 3.
778 *Nature* **630**, 493–500 (2024).

779 34. Jumper, J. *et al.* Highly accurate protein structure prediction with AlphaFold. *Nature* 1–7 (2021)
780 doi:10.1038/s41586-021-03819-2.

781 35. Gautier, R., Douguet, D., Antonny, B. & Drin, G. HELIQUEST: a web server to screen sequences
782 with specific alpha-helical properties. *Bioinformatics* **24**, 2101–2102 (2008).

783 36. Beeman, N., Sapre, T., Ong, S.-E. & Yadav, S. Neurodevelopmental disorder–associated mutations in
784 TAOK1 reveal its function as a plasma membrane remodeling kinase. *Sci Signal* **16**, eadd3269 (2023).

785 37. Kerkhofs, M. *et al.* The AMPK-related kinase NUAK1 regulates neuronal morphogenesis through the
786 RNA splicing co-factor SON. *bioRxiv* 2025.10.10.681550 (2025) doi:10.1101/2025.10.10.681550.

787 38. Hertz, N. T. *et al.* Chemical genetic approach for kinase-substrate mapping by covalent capture of
788 thiophosphopeptides and analysis by mass spectrometry. *Curr Protoc Chem Biol* **2**, 15–36 (2010).

789 39. Blethrow, J. D., Glavy, J. S., Morgan, D. O. & Shokat, K. M. Covalent capture of kinase-specific
790 phosphopeptides reveals Cdk1-cyclin B substrates. *Proc. Natl. Acad. Sci. U.S.A.* **105**, 1442–1447 (2008).

791 40. Blethrow, J., Zhang, C., Shokat, K. M. & Weiss, E. L. Design and use of analog-sensitive protein
792 kinases. *Curr Protoc Mol Biol* **Chapter 18**, Unit 18.11-18.11.19 (2004).

793 41. Yadav, S. *et al.* TAOK2 Kinase Mediates PSD95 Stability and Dendritic Spine Maturation through
794 Septin7 Phosphorylation. *Neuron* **93**, 379–393 (2017).

795 42. Johnson, J. L. *et al.* An atlas of substrate specificities for the human serine/threonine kinome. *Nature*
796 **613**, 759–766 (2023).

797 43. Fukaya, M., Ohta, S., Hara, Y., Tamaki, H. & Sakagami, H. Distinct subcellular localization of
798 alternative splicing variants of EFA6D, a guanine nucleotide exchange factor for Arf6, in the mouse
799 brain. *J. Comp. Neurol.* **524**, 2531–2552 (2016).

800 44. Gonzalez, D. A. *et al.* The Arf6 activator Efa6/PSD3 confers regional specificity and modulates
801 ethanol consumption in Drosophila and humans. *Mol. Psychiatry* **23**, 621–628 (2018).

802 45. Kanamarlapudi, V. Exchange Factor EFA6R Requires C-terminal Targeting to the Plasma Membrane
803 to Promote Cytoskeletal Rearrangement through the Activation of ADP-ribosylation Factor 6 (ARF6)*. *J.*
804 *Biol. Chem.* **289**, 33378–33390 (2014).

805 46. Macia, E. *et al.* The C-terminal domain of EFA6A interacts directly with F-actin and assembles F-
806 actin bundles. *Sci. Rep.* **9**, 19209 (2019).

807 47. Fukaya, M., Ohta, S., Hara, Y., Tamaki, H. & Sakagami, H. Distinct subcellular localization of
808 alternative splicing variants of EFA6D, a guanine nucleotide exchange factor for Arf6, in the mouse
809 brain. *J. Comp. Neurol.* **524**, 2531–2552 (2016).

810 48. Banerjee, S. *et al.* Interplay between Polo kinase, LKB1-activated NUAK1 kinase, PP1βMYPT1
811 phosphatase complex and the SCFβTrCP E3 ubiquitin ligase. *Biochem. J.* **461**, 233–245 (2014).

812 49. Kim, Y. *et al.* ADP-ribosylation Factor 6 (ARF6) Bidirectionally Regulates Dendritic Spine
813 Formation Depending on Neuronal Maturation and Activity*. *J. Biol. Chem.* **290**, 7323–7335 (2015).

814 50. Choi, S. *et al.* ARF6 and EFA6A Regulate the Development and Maintenance of Dendritic Spines. *J.*
815 *Neurosci.* **26**, 4811–4819 (2006).

816 51. Brown, F. D., Rozelle, A. L., Yin, H. L., Balla, T. & Donaldson, J. G. Phosphatidylinositol 4,5-
817 bisphosphate and Arf6-regulated membrane traffic. *J. Cell Biol.* **154**, 1007–1018 (2001).

818 52. Naslavsky, N., Weigert, R. & Donaldson, J. G. Convergence of Non-clathrin- and Clathrin-derived
819 Endosomes Involves Arf6 Inactivation and Changes in Phosphoinositides. *Mol. Biol. Cell* **14**, 417–431
820 (2003).

821 53. Mezache, L. & Leterrier, C. Advancing Super-Resolution Microscopy: Recent Innovations in
822 Commercial Instruments. *Microsc. Microanal.* **31**, ozaf004 (2025).

823 54. Eyck, L. F. T., Taylor, S. S. & Kornev, A. P. Conserved spatial patterns across the protein kinase
824 family. *Biochim. Biophys. Acta (BBA) - Proteins Proteom.* **1784**, 238–243 (2008).

825 55. Kennedy, E. J., Yang, J., Pillus, L., Taylor, S. S. & Ghosh, G. Identifying Critical Non-Catalytic
826 Residues that Modulate Protein Kinase A Activity. *PLoS ONE* **4**, e4746 (2009).

827 56. Zhou, X. *et al.* Integrating de novo and inherited variants in 42,607 autism cases identifies mutations
828 in new moderate-risk genes. *Nat. Genet.* **54**, 1305–1319 (2022).

829 57. Jaworski, J. ARF6 in the nervous system. *Eur. J. Cell Biol.* **86**, 513–524 (2007).

830 58. Mancina, R. M. *et al.* PSD3 downregulation confers protection against fatty liver disease. *Nat. Metab.*
831 **4**, 60–75 (2022).

832 59. Sheng, M. *et al.* NUAK1 promotes metabolic dysfunction-associated steatohepatitis progression by
833 activating Caspase 6–driven pyroptosis and inflammation. *Hepatol. Commun.* **8**, e0479 (2024).

834 60. Chen, P., Li, K., Liang, Y., Li, L. & Zhu, X. High NUAK1 expression correlates with poor prognosis
835 and involved in NSCLC cells migration and invasion. *Exp. Lung Res.* **39**, 9–17 (2013).

836 61. Jin, L. *et al.* PSD3 is an oncogene that promotes proliferation, migration, invasion, and G1/S
837 transition while inhibits apoptotic in papillary thyroid cancer. *J. Cancer* **12**, 5413–5422 (2021).

838 62. Luo, S. *et al.* PSD3 as a context-dependent modulator of immune landscape and tumor aggressiveness
839 in esophageal squamous cell carcinoma. *Front. Immunol.* **16**, 1641254 (2025).

840 63. Byeon, S. *et al.* TAOK2 drives opposing cilia length deficits in 16p11.2 deletion and duplication
841 carriers. *Stem Cell Rep.* **20**, 102608 (2025).

842 64. Kong, A. T., Leprevost, F. V., Avtonomov, D. M., Mellacheruvu, D. & Nesvizhskii, A. I. MSFragger:
843 ultrafast and comprehensive peptide identification in mass spectrometry–based proteomics. *Nat. Methods*
844 **14**, 513–520 (2017).

845 65. Demichev, V., Messner, C. B., Vernardis, S. I., Lilley, K. S. & Ralser, M. DIA-NN: Neural networks
846 and interference correction enable deep proteome coverage in high throughput. *Nat. methods* **17**, 41–44
847 (2020).

848

## FIGURE LEGENDS

**Figure 1. Autism-associated NUAK1 mutations impact catalytic activity and subcellular localization**

**(a)** Day *in vitro* (div) 14 rat hippocampal neurons stained with antibodies against NUAK1 and MAP2, with nuclear marker DAPI. Right panels show magnified soma with anti-NUAK1 and either MAP2 (top panel) or DAPI (bottom panel). Error bars represent 20μm in full images and 10μm in zoomed images at right. **(b)** Human brain transcriptomic data for NUAK1 obtained from Human Brain Transcriptome (HBT) database across different stages of human brain development. Genome-wide, exon-level transcriptome data in HBT was generated using the Affymetrix GeneChip Human Exon 1.0 ST Arrays from over 1,340 tissue samples sampled from both hemispheres of postmortem human brains. Specimens range from embryonic development to adulthood (periods 1-15) and represent both males and females. Brain regions plotted are the neocortex (NCX), hippocampus (HIP), amygdala (AMY), striatum (STR), mediodorsal nucleus of the thalamus (MD), and cerebellar cortex (CBC). **(c)** *In situ* hybridization data from the Allen Brain Atlas using antisense probe against NUAK1 on sagittal sections of postnatal day 56 (P56) C57BL6/J male mouse brain. Scale bar represents 839μm. **(d)** Two-dimensional schematic of NUAK1 protein domains, with the N-terminal kinase domain, 3 GILK motifs, and C-terminal amphipathic helix indicated with colored boxes. The three NUAK1 ASD-associated mutations are shown with lollipops above the protein domains: the two missense mutations Q161E and A653V, and the early truncation mutation Q433ter (Q433*). **(e)** ConSurf evolutionary conservation analysis of the two ASD-associated

23 missense mutations in NUAK1: Q161E and A653V. Residues are colored according to
24 their evolutionary conservation, with warm colors indicating conserved residues and cool
25 colors indicating variable residues. **(f)** Heliquest-predicted amphipathic helix at the C-
26 terminus of NUAK1, which spans amino acids 644-661. Alanine 653, the site of the A653V
27 ASD-associated mutation, is indicated. The arrow indicates the hydrophobic face of the
28 amphipathic helix. **(g)** Western blot of immunoprecipitated GFP-NUAK1 mutants
29 incubated plus/minus ATP to allow NUAK1 to autophosphorylate. Immunoblots show anti-
30 phospho-serine/threonine and anti-GFP (loading control). **(h)** Quantification of kinase
31 activity of NUAK1 mutants, with the phospho-serine/threonine signal divided by the GFP
32 loading control and all samples normalized as a percentage of WT + ATP per experiment
33 (n=3 independent experiments, ** denotes $p<0.005$; *** denotes $p<0.001$, one way
34 ANOVA with Tukey's multiple comparisons). All error bars represent standard error of the
35 mean. **(i)** DIV 14 rat embryonic hippocampal neurons expressing GFP-tagged NUAK1
36 mutants and membrane marker myristoyl-tdtomato (myr-tdtomato). Neurons were
37 transfected with GFP-NUAK1 and myr-tdTomato on DIV 12 and fixed 48 hours later. The
38 arrowhead in Q433* image indicates the predominantly nuclear localization of this
39 mutation. Scale bar represents 20µm in all images.
40

41 **Figure 2. Engineering ATP-analog sensitive NUAK1 kinase through the gatekeeper**
42 **residue mutation M132G**

43 **(a**) Multiple sequence alignment of the kinase domains of serine/threonine kinases,
44 including NUAK1, NUAK1, AMPKα2, MST3, and TAOK2. The conserved methionine

45 gatekeeper residue is colored red and underlined, while the flanking residues are colored
46 blue. The four highly conserved residues surrounding the gatekeeper are indicated with
47 a box. **(b)** Top: bulky side groups (benzyl, phenyl, and furfuryl) that are N6-substitutents
48 of ATPγS (right) in kinase assays. Bottom: Western blots showing utilization of bulky
49 ATPγS molecules by purified HM-tagged NUAK1 (amino acid 1-433). Antibody against
50 phosphothioester (pTE) is used as a readout of autophosphorylation, while anti-His is
51 used as a loading control. The optimal gatekeeper mutant/bulky ATPγS combination of
52 M132G NUAK1 and furfuryl-ATPγS is indicated with a red box. **(c)** Quantification of
53 utilization of bulky ATPγS analogs by HM-NUAK1, with pTE signal divided by loading
54 control His for each sample. Data were normalized to WT for each analog, with KD and
55 MG represented as a ratio of WT. N=3 independent experiments. Error bars represent
56 standard error of the mean. **(d)** HA-tagged full-length NUAK1 KD or MG was expressed
57 in HEK293T cells followed by lysis and immunoprecipitation for the indicated time.
58 Immunoprecipitated NUAK1 was incubated with mouse brain lysate and furfuryl ATPγS,
59 followed by alkylation to generate phosphothioester for WB detection. HA is used as a
60 loading control for NUAK1, while phosphothioester (pTE) is used as a readout of
61 substrate phosphorylation in mouse brain lysate. **(e)** Schematic of labeling of mouse brain
62 lysate by analog-sensitive (AS) NUAK1 and N6-furfuryl-ATPγS (reaction 1), or negative
63 control K84M (KD) NUAK1 and N6-furfuryl-ATPγS (reaction 2). Thiophosphorylated
64 substrate proteins were digested with trypsin, and thiophosphorylated peptides were then
65 covalently captured using iodoacetamide (IAA) beads. Beads were treated with oxone to
66 specifically elute off thiophosphorylated peptides as phosphopeptides, while peptides

67 with other thiol groups (e.g., cysteines) are retained on the beads. The resulting
68 phosphopeptides are then analyzed by LC-MS/MS.
69
70 **Figure 3. NUAK1 phosphorylation targets identified by chemical-genetic screen**
71 **(a)** Putative NUAK1 substrate proteins (31 total) that occurred in at least 3/5 analog
72 sensitive samples and 0/5 kinase dead samples were analyzed for their roles in
73 endocytosis, splicing, cytoskeletal reorganization, as well as development of dendrites,
74 axons, or synapses. Each substrate is color-coded according to its role(s) in each of these
75 processes, with light green for endocytosis, teal for splicing, yellow for cytoskeleton, pink
76 for axon, and blue for dendrites, with the legend in the lower right panel showing each
77 individual color. Substrates with roles in synaptic development are located in the "synapse"
78 box on the middle right. Substrates with multiple functions are indicated with gradients
79 with 2-4 colors. **(b)** The 9 amino acids surrounding the phosphoacceptor (from residues -
80 5 to +4) for the 31 potential substrates of NUAK1 that occurred in at least 3/5 analog
81 sensitive samples and 0/5 kinase dead samples were analyzed using the Phosphosite.org
82 Weblogo tool to generate a preference map for NUAK1 substrate phosphorylation. **(c)**
83 Putative NUAK1 substrate proteins that occurred in at least 3/5 analog sensitive samples
84 and 0/5 kinase dead samples were analyzed for how well they fit the established NUAK1
85 consensus sequence. Most stringently, NUAK1 requires a basic residue (K/R) at the -3
86 position. After filtering the 31 unique potential substrates by this stringent consensus
87 sequence, 17 putative substrates remained. The mouse Uniprot ID and protein name for
88 each protein is listed, as are the human and mouse phosphosites. The amino acids

89 surrounding the phosphosite are listed in this table, from the -5 position to the +4 position
90 relative to the phosphoacceptor. Based on the established NUAK1 consensus sequence,
91 along with the data from our MS runs, we were able to establish the optimal motif for
92 substrate phosphorylation by NUAK1. This optimal motif: (1) contains a basic residue at
93 -3 position; (2) contains a serine at -2 position; (3) contains a serine phosphoacceptor;
94 and (4) contains an aliphatic branched chain amino acid at -5 and +4 positions. Residues
95 are color coded based on whether the residue fits the optimal NUAK1 motif at the given
96 site, with positions -5 and +4 in purple, positions -4, -3, and -1 in cyan, and positions -2,
97 +1, +2, and +3 in chartreuse. The central phosphoacceptor at position 0 is colored in dark
98 green for serine (more preferred) and light green for threonine (less preferred).

99 **Figure 4. PSD3 is a bona fide direct phosphorylation target of NUAK1 kinase.**
100 **(a)** Two-dimensional schematic representation of the function domains of PSD3 isoform
101 1 (Uniprot # Q9NYI0), isoform 3 (Uniprot # Q9NYI0-3), and the shortened PSD3 construct
102 used for biochemical experiments, PSD3 CC tail. PSD3 isoforms 1 and 3 share the same
103 3 conserved functional domains, including a Sec7 GEF domain (green) which activates
104 ARF6, Pleckstrin Homology (PH) domain with specificity for PI(4,5)P2, and a Coiled Coil
105 (CC) domain which binds to actin. The MS-identified phosphosite on PSD3, S1011 in
106 isoform 1 or S476 in isoform 3, is indicated with a lollipop. The shortened CC tail domain
107 used for protein purification contains an N-terminal GST tag followed by the C-terminal
108 region of PSD3, from the CC domain to the end of the protein containing the S476/S1011
109 phosphosite. **(b)** ConSurf evolutionary conservation analysis of the MS-identified
110 phosphosite of PSD3, S1011 in isoform 1 or S476 in isoform 3. The S1011

111 phosphoacceptor residue is boxed in violet. Residues are colored according to their
112 evolutionary conservation, with warmer colors indicating conserved residues and cool
113 colors indicating variable residues. **(c)** V5-tagged PSD3 isoform 3 WT or S476A was
114 immunoprecipitated from HEK293T cells, followed by incubation with purified HM-NUAK1
115 WT and ATP. Immunoblots show V5 as a loading control for PSD3 and His as a control
116 for NUAK1, and phospho-serine/threonine as a readout of phosphorylation for both
117 NUAK1 and PSD3 at their respective molecular weights. **(d)** Quantification of
118 phosphorylation of PSD3 by NUAK1, as measured by phospho-serine/threonine divided
119 by V5 signal. Each experiment is normalized to WT PSD3, with S>A PSD3 as a ratio of
120 WT signal (n=3 independent experiments; *** denotes $p<0.001$, student's t-test). Error
121 bars represent standard error of the mean. **(e)** HEK293T cells were co-transfected with
122 mCherry-V5-PSD3 isoform 3 and either HA-empty vector or HA-NUAK1 WT. Cells were
123 then lysed, and protein was immunoprecipitated using HA beads. Immunoblots show HA
124 signal for HA-empty vector or HA-NUAK1, and V5 signal for mCherry-V5-PSD3. **(f)**
125 Quantification of V5 signal for input and HA IP for n=3 independent experiments. Error
126 bars represent standard error of the mean; ** denotes $p<0.005$, one way ANOVA with
127 Tukey's multiple comparisons. **(g)** HEK293T cells were co-transfected with mCherry-V5-
128 PSD3 isoform 3 and either HA-empty vector or HA-NUAK1 WT. Cells were then lysed,
129 and protein was immunoprecipitated using V5 beads. Immunoblots show HA signal for
130 HA-empty vector or HA-NUAK1, and V5 signal for mCherry-V5-PSD3. **(h)** Quantification
131 of HA signal for input and V5 IP, for n=3 independent experiments. Error bars represent
132 standard error of the mean; * denotes $p<0.05$, one way ANOVA with Tukey's multiple

133 comparisons. **(i)** HM-NUAK1 WT or KD was incubated with GST-PSD3-CC tail WT or
134 S>A in the presence of $Mg^{2+}$ and ATPγS, followed by alkylation with PNBM to generate
135 thiophosphate esters as a readout of thiophosphorylation by NUAK1. **(j)** Quantification of
136 phosphorylation of GST-PSD3-CC tail WT or S>A by HM-NUAK1 WT or KD. Data are
137 normalized to WT PSD3 + WT HM-NUAK1 for each experiment, with all other samples
138 as a percentage of WT/WT (n=3 independent experiments; **** indicates $p<0.0001$, one
139 way ANOVA with Tukey's multiple comparisons). Error bars represent standard error of
140 the mean **(k)** Alphafold-predicted structure of NUAK1 WT (Uniprot # O60285) with the
141 previously identified and validated substrate MYPT1 (Uniprot ID #O14974), along with
142 adaptor protein Protein Phosphatase 1 beta (Uniprot ID #P62140). NUAK1 kinase domain
143 is displayed as an electrostatic surface representation, with red-toned colors representing
144 a negative charge, and blue-toned colors representing a positive charge. MYPT1 is
145 colored in light blue, and amino acids within the NUAK1 substrate binding groove are
146 color coded according to their position and side chain, with Leu at -5 and +4 in limon,
147 Lys/His at -4, -3, and -1 in blue, and central phospho-acceptor Ser in green. Amino acid
148 side chains are shown for positions -5 to +4 surrounding the MYPT1 S445 phosphosite.
149 **(l)** Alphafold3 predicted structure of NUAK1 WT (Uniprot # O60285) with PSD3 isoform 1
150 WT (Uniprot # Q9NYI0), following the same color scheme as figure 4k. Amino acid side
151 chains are shown for positions -5 to +4 surrounding the PSD3 S476 phosphosite.
152
153 **Figure 5. Phosphorylation of PSD3 at S476 regulates ARF6 dependent trafficking**

154 **(a)** HEK393T cells co-expressing mCherry-tagged WT or dominant negative T44N ARF6
155 (magenta) and sfGFP-tagged WT-PSD3, Sec7 mutant E114K or phosphomutant S476A
156 (green). Scale bar is 5μm. **(b)** Area of intracellular vesicles positive for ARF6 and PSD3
157 normalized to the total cell area is plotted for each condition (n>20 cells from 3
158 experiments, ** denotes p<0.005 and **** indicates p<0.0001, one-way ANOVA with
159 Tukey's multiple comparisons). **(c)** HEK393T cells co-expressing the PI(4,5)P2 sensor
160 EGFP-PLCD1 (gray) along with either mCherry-tagged WT or phosphomutant PSD3
161 S476A (red). Scale bar is 5μm. **(d)** Area of intracellular vesicles positive for PI(4,5)P2
162 sensor PH-PLCD1 normalized to the total cell area is plotted for each condition (n>23
163 cells from 3 experiments, **** indicates p<0.0001, unpaired t-test with Welch's correction).
164 All error bars are standard error of the mean.
165
166 **Figure 6. NUAK1 mediated PSD3 phosphorylation at S476 restricts maturation of**
167 **filopodia into dendritic spines**
168 **(a)** Representative images of DIV13 rat embryonic hippocampal neurons co-expressing
169 membrane marker myristoylated-tdTomato (red) along with either sfGFP-tagged wildtype
170 (WT) PSD3 or phosphomutant S476A (cyan). Scale bar is 10mm. **(b)** Magnified insets
171 are shown to highlight the morphology of dendritic spines and the enrichment for PSD3
172 within spines. Grayscale and pseudocolored images show intensity of PSD3 distribution
173 in WT and S476 conditions. Scale bar is 1μm. **(c)** Quantification of percent spines
174 enriched in PSD3 in hippocampal neurons expressing WT-PSD3 and S476A
175 phosphomutant (n>15 neurons for each condition from three experiments, **** denotes

176 p<0.0001, t-test with Welch's correction). **(d)** Protrusion density per micron dendrite
177 length is plotted for neurons expressing WT-PSD3 and S476A phosphomutant (n>55
178 neurons for each condition from three experiments, ns denotes p>0.05, t-test with Welch's
179 correction). **(e)** Percent protrusions classified into stubby, thin, filopodia and mushrooms
180 spines are plotted neurons expressing WT-PSD3 and S476A phosphomutant (n>55
181 neurons for each condition from three experiments, **** denotes p<0.0001 and * denotes
182 p<0.05, 2-way ANOVA with multiple comparisons). All error bars are standard error of the
183 mean. **(f)** Schematic depicts working model based on the results showing role of NUAK1
184 phosphorylation of PSD3 in regulation of ARF6 mediated membrane internalization and
185 PI(4,5)P2 production. Role of PSD3 phosphorylation in maturation of dendritic spines
186 through ARF6 is shown.
187
188 **Figure 7. NUAK1 phosphorylation targets in neuronal development and disease**
189 **(a)** Schematic shows substrates of NUAK1 identified by the chemical genetic screen
190 which are binned by their roles in axonal, dendritic, and synaptic development, as well as
191 splicing. Each substrate is color-coded according to its known function(s), with light green
192 for endocytosis, teal for splicing, yellow for cytoskeleton, pink for axon, and blue for
193 dendrites, with the legend in the lower left panel showing each individual color. Substrates
194 with multiple functions are indicated with gradients of 2-4 colors. **(b)** Schematic
195 representation of the role of PSD3 and NUAK1 in ARF6 activation. At the plasma
196 membrane, PSD3 recruits inactive, GDP-bound ARF6. PSD3 exchanges GDP for GTP,
197 generating active ARF6, which promotes the formation of PI(4,5)P2. This increase in PIP2

198 causes internalization of PSD3 and ARF6 on PIP2-enriched vesicles. In normal conditions,
199 Rab5, ARF6 GAPs, and lipid phosphatases are recruited to these vesicles, leading to a
200 cessation of ARF6 activity and depletion of PIP2. These vesicles can then continue in the
201 endolysosomal pathway, or be recycled to the cell surface. When NUAK1 is not present,
202 or when the PSD3 S476 phosphosite is mutated to alanine, ARF6 remains active and
203 bound to GTP, accumulating in large, PIP2-enriched vesicles. **(c)** Schematic of the role
204 of PSD3 in dendritic spine maturation. PSD3 activation of ARF6 leads to an increased
205 proportion of mature, mushroom-shaped dendritic spines and a corresponding loss of
206 immature filopodia. In normal conditions, PSD3 is phosphorylated by NUAK1, keeping
207 ARF6 activation in check. When NUAK1 is inactive or when the PSD3 phosphosite is
208 mutated to alanine, PSD3 phosphorylation is lost, leading to an aberrant increase in the
209 proportion of active ARF6.

# Chemical Genetic Screen Identifies PSD3 as a Direct Substrate of NUAK1 that Regulates Dendritic Spine Maturation

Josilyn R. Sejd[1], Daphnée M. Marciniak[1], Moira A. Cornell[1], Angel Sondhi[1], Shao-En Ong[1] and Smita Yadav[1,2*]

[1]Department of Pharmacology, University of Washington, Seattle, United States.
[2]Institute of Stem Cell and Regenerative Medicine, Seattle, United States
* Corresponding author

## Supplementary materials

**Figure S1:** NUAK1 structure and localization in mitotically active cells

**Figure S2:** NUAK1 chemical genetic method development

**Figure S3:** PSD3 evolutionary conservation and purification from *E. coli*

**Table S4:** Excel spreadsheet with 3 sheets. Sheet 1 contains an index and definitions of column titles. Sheet 2 contains curated proteins which occurred in 3/5 M132G replicates and 0/5 KD replicates and fit stringent consensus of K/R at -3 position. Sheet 3 contains all proteins identified in LC-MS/MS-based chemical genetic screen

## Supplemental Figure Legends

### Figure S1: NUAK1 structure and localization in mitotically active cells

**(a)** Alphafold-predicted structure for NUAK1 (AF-O60285-F1-v6), visualized in Pymol viewer. Color scheme reflects pLDDT value per residue, with dark blue representing very high confidence (>90%), cyan representing high confidence (70-90%), yellow representing low confidence (50-70%), and orange representing very low confidence

30 (<50%). The C-terminal helix containing Alanine 653 is labeled as “A653”. Dashed box
31 represents the region that is magnified in S1b.
32 **(b)** Left: Zoom on the kinase domain of NUAK1 with unstructured domains hidden,
33 showing the position of the A653-containing helix relative to the kinase domain. Dashed
34 box shows area which is magnified in the right panel. Right: Zoom on the NUAK1 C-
35 terminal alpha helix containing Alanine 653, with A653 shown in licorice stick format.
36 **(c)**GFP-tagged NUAK1 mutants were expressed in human neural progenitor cells
37 (NPCs), followed by fixation and staining with anti-SC35 antibody and DAPI. Panels
38 show, from top to bottom, GFP-NUAK1, SC35 staining, merge of GFP-NUAK1, SC35,
39 and DAPI with a dashed box around the nucleus, and magnified nuclear area with merge
40 of GFP-NUAK1 and SC35.
41
42 **Figure S2: NUAK1 chemical genetic method development**
43 **(a)** Purification of HM-NUAK1 1-433 WT from *E. coli*. HM-NUAK1 1-433 WT was
44 expressed in *E. coli*, followed by induction with IPTG and lysis. Coomassie stain shows
45 protein gel with ladder of indicated molecular weights, with HM-NUAK1 1-433 WT
46 purification. Samples show pre-induction, whole cell lysate post sonication, supernatant
47 and pellet following centrifugation post sonication, flow through from bead binding, elution
48 1, HisPur beads following elution, and elution after incubation with SP beads. **(b)**
49 Purification of HM-NUAK1 1-433 WT from *E. coli* with the same samples loading as in (c),
50 with IB against His tag. **(c)** Purification of HM-NUAK1 1-433 KD and M132G from *E. coli*,
51 with samples from the first elution (E1), flow through after binding to SP beads (FT), wash

52 1 after binding to SP beads, and purified protein after elution from SP beads (final), with
53 purification process shown for both KD and M132G HM-NUAK1 1-433, with final WT HM-
54 NUAK1 1-433 (lane 9) shown for reference. A red dashed box indicates the relevant
55 bands. **(d)** Western blot of full-length HA-NUAK1 WT, K84M (KD), M132A, and M132G
56 incubated with the indicated ATPγS analogs and Mg2+ to allow autophosphorylation,
57 followed by alkylation of thiophosphates with pNBM to generate thiophosphate esters
58 (pTE). Anti-HA is used as a loading control, while pTE is used as a readout of
59 autophosphorylation. **(e)** Quantification of utilization of N6-bulky ATPγS analogs by HA-
60 NUAK1, with pTE signal divided by loading control His for each sample. Error bars
61 represent standard error of the mean.
62
63 **Figure S3: PSD3 evolutionary conservation and purification from *E. coli***
64 **(a)** The sequences for human PSD3 (NP_056125.3) and 457 orthologs were obtained
65 from the NCBI gene browser, followed by alignment using Cobalt. Multiple sequence
66 alignments were visualized using SnapGene viewer. Amino acids L995 to D1017 in
67 human PSD3 are shown, with the height and color of each bar corresponding to
68 percentage conservation of that residue in the 457 orthologs analyzed. The consensus
69 amino acid sequence is listed, with X indicating a lack of conservation of one specific
70 amino acid at a given site. The phosphosite on PSD3 that was identified by MS is
71 indicated with an asterisk, and the flanking residues from -5 to +4 are surrounded by a
72 dashed box. The legend shows the color scheme based on percentage conservation of
73 the indicated amino acid, with >88% conservation in dark red, 80-87% in red, 63-79% in

74 orange, 50-64% in yellow-orange, and <49% in light blue. **(b)** GST-PSD3-CC tail (WT or
75 S476A) was expressed in *E. coli*, followed by induction with IPTG and lysis. Coomassie
76 stain shows protein gel with ladder of indicated molecular weights, with GST-PSD3-CC
77 tail purification. Samples show pre-induction, 1 and 2 hours post IPTG induction, whole
78 cell lysate post sonication, supernatant and pellet following centrifugation post sonication,
79 flow through from bead binding, elutions 1-6 (E1-6), and glutathione beads following 6
80 elutions with 25mM glutathione. The relevant bands are indicated with a dashed red box.

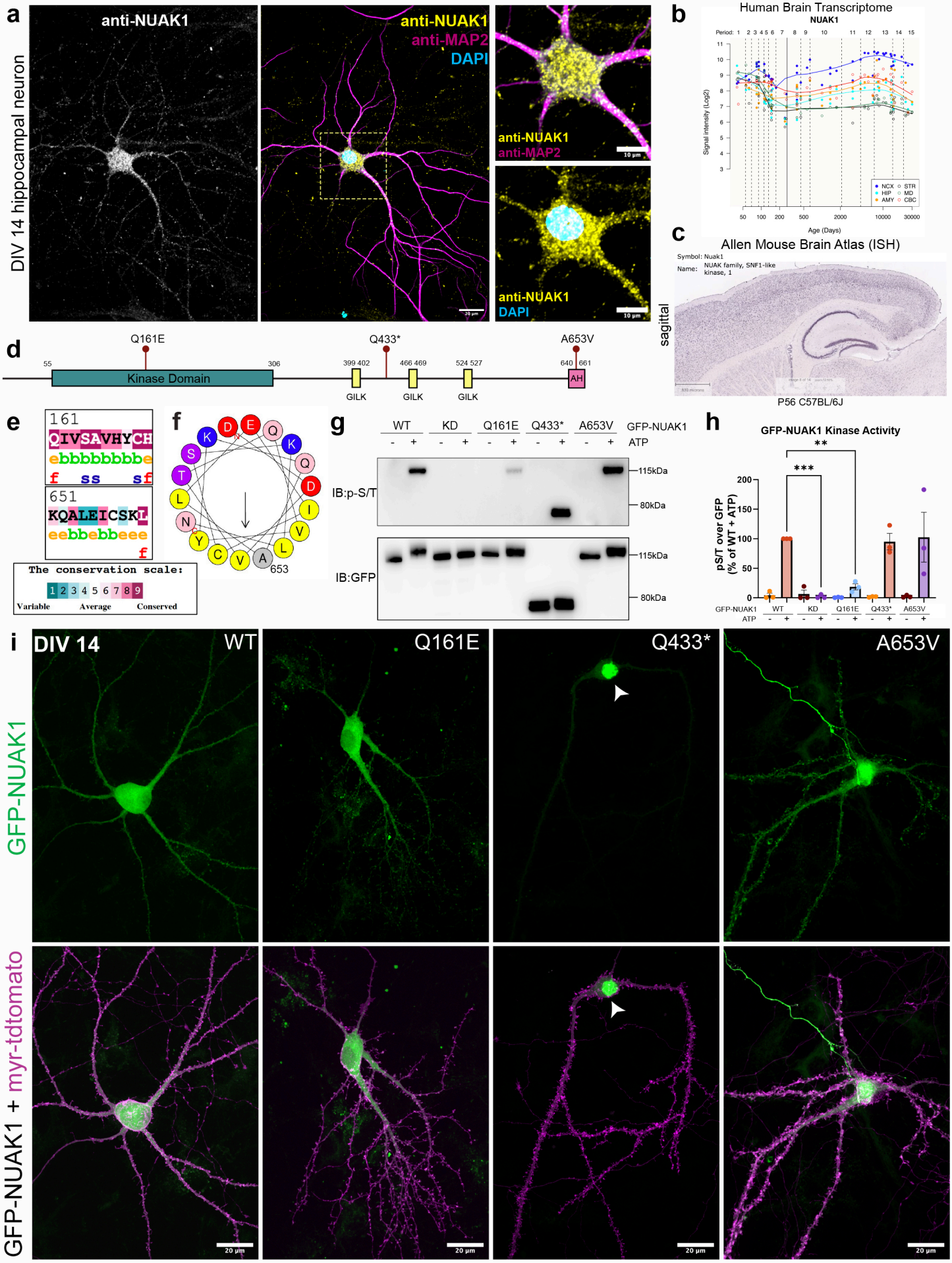
a
DIV 14 hippocampal neuron
anti-NUAK1
anti-NUAK1
anti-MAP2
DAPI
anti-NUAK1
anti-MAP2
anti-NUAK1
DAPI
b
Human Brain Transcriptome
NUAK1
Signal intensity (Log2)
Age (Days)
NCX
STR
HIP
MD
AMY
CBC
c
Allen Mouse Brain Atlas (ISH)
Symbol: Nuak1
Name: NUAK family, SNF1-like kinase, 1
sagittal
P56 C57BL/6J
d
Q161E
Q433*
A653V
Kinase Domain
GILK
GILK
GILK
AH
e
161
QIVSAVHYCH
653
KQALEICSKL
The conservation scale:
Variable
Average
Conserved
f
653
g
WT
KD
Q161E
Q433*
A653V
GFP-NUAK1
ATP
IB:p-S/T
IB:GFP
115kDa
80kDa
h
GFP-NUAK1 Kinase Activity
pS/T over GFP (% of WT + ATP)
i
DIV 14
WT
Q161E
Q433*
A653V
GFP-NUAK1
GFP-NUAK1 + myr-tdtomato
20 µm

**Figure 1**

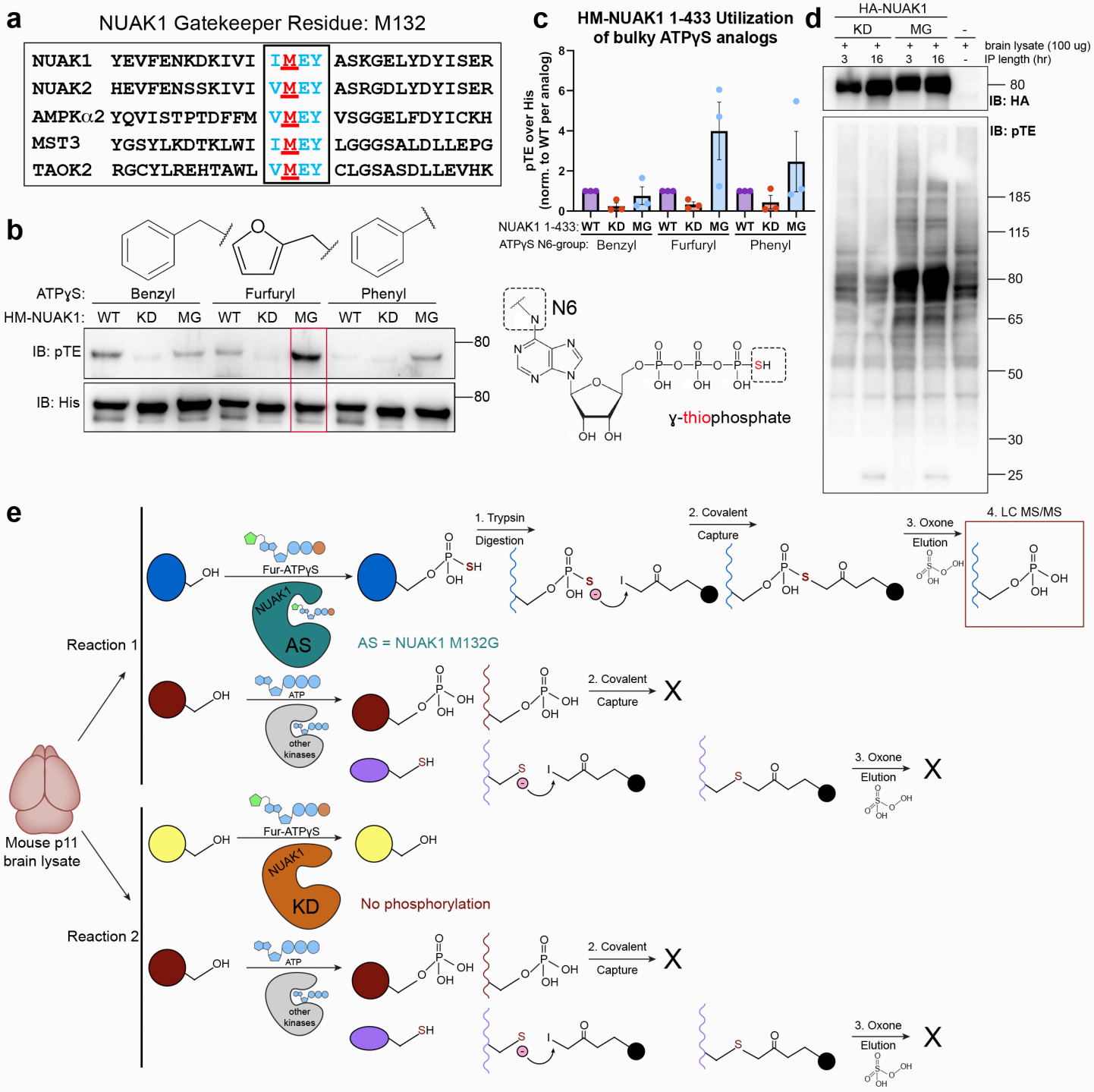
a
NUAK1 Gatekeeper Residue: M132
NUAK1 YEVFENKDKIVI IMEY ASKGELYDYISER
NUAK2 HEVFENSSKIVI VMEY ASRGDLYDYISER
AMPKα2 YQVISTPTDFFM VMEY VSGGELFDYICKH
MST3 YGSYLKDTKLWI IMEY LGGGSALDLLEPG
TAOK2 RGCYLREHTAWL VMEY CLGSASDLLEVHK
b
ATPγS: Benzyl Furfuryl Phenyl
HM-NUAK1: WT KD MG WT KD MG WT KD MG
IB: pTE
IB: His
80
80
c
HM-NUAK1 1-433 Utilization of bulky ATPγS analogs
pTE over His (norm. to WT per analog)
NUAK1 1-433: WT KD MG WT KD MG WT KD MG
ATPγS N6-group: Benzyl Furfuryl Phenyl
N6
γ-thiophosphate
d
HA-NUAK1
KD MG -
brain lysate (100 ug)
IP length (hr)
IB: HA
IB: pTE
80
185
115
80
65
50
30
25
e
Reaction 1
Reaction 2
Mouse p11 brain lysate
Fur-ATPγS
ATP
other kinases
NUAK1
AS
KD
AS = NUAK1 M132G
No phosphorylation
1. Trypsin Digestion
2. Covalent Capture
3. Oxone Elution
4. LC MS/MS
X

Figure 2

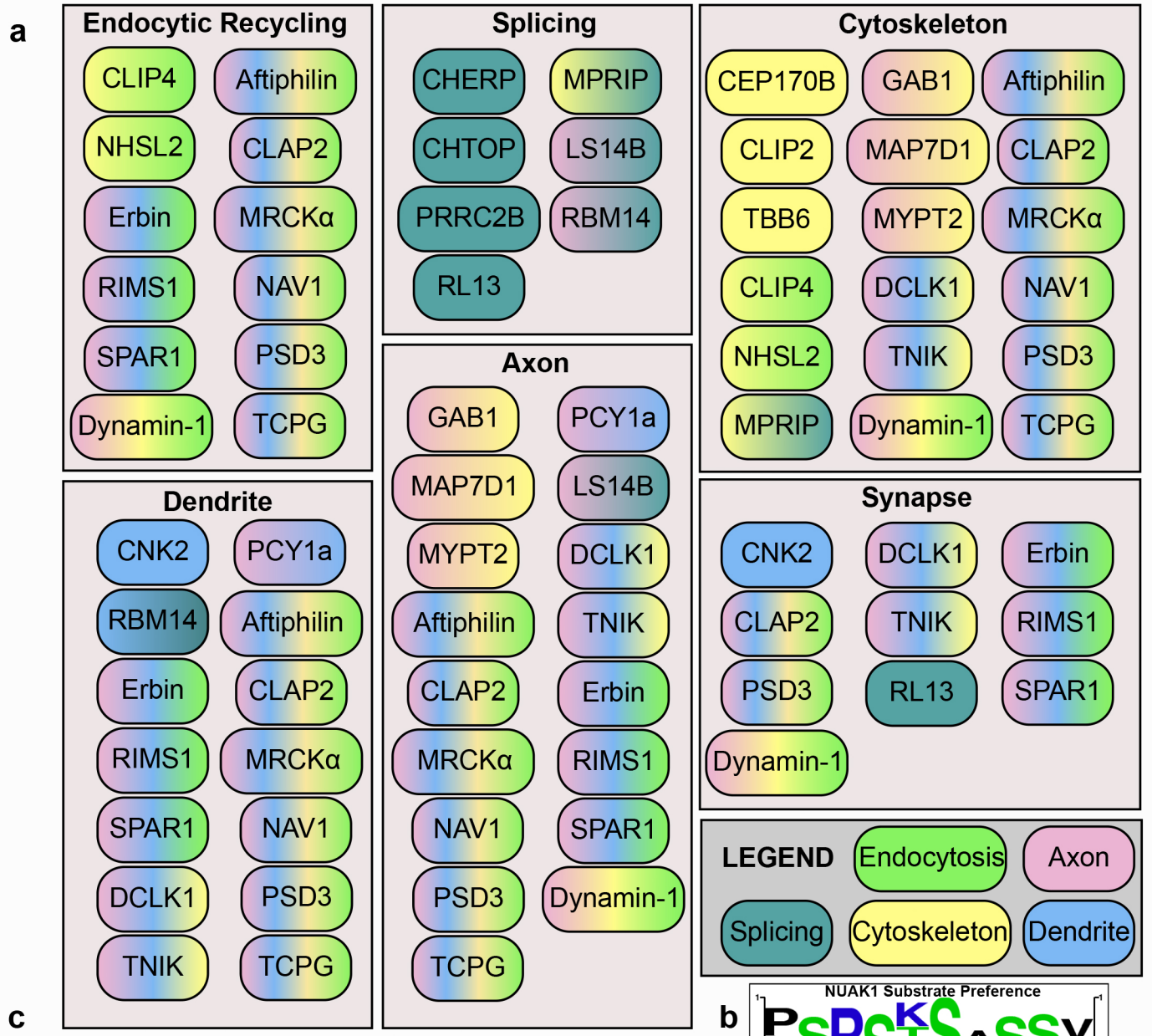


c

| Site | -5 | -4 | -3 | -2 | -1 | 0 | +1 | +2 | +3 | +4 |
|---|---|---|---|---|---|---|---|---|---|---|
| Optimal motif | P | K | R | S | K/R/H | S | A | S/T | S | L/V |
| Secondary | L/I | R | K | X | P | S | S | X | X | S |
| Additional | R | S | X | X | T | T | X | X | X | X |

b

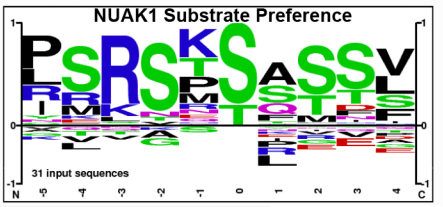


| Mouse ID | Protein name | human site | mouse site | -5 | -4 | -3 | -2 | -1 | S/T | +1 | +2 | +3 | +4 | Localization (Uniprot) |
|---|---|---|---|---|---|---|---|---|---|---|---|---|---|---|
| Q2PFD7 | PSD3 | S1011 | S1000 | L | K | K | S | H | S | S | P | S | L | Membrane, cytosol |
| A2AJI0 | MAP7D1 | S313 | S315 | L | A | R | S | R | S | A | V | T | L | Cytosol |
| Q80U49 | CEP170B | S1364 | S1349 | P | T | R | S | P | S | L | G | N | V | Cytosol |
| P83510 | TNIK | S570 | S541 | P | P | R | S | E | S | F | S | I | S | Nucleus, cytosol |
| Q0PHV7 | DACT3 | S426 | S409 | A | A | R | S | Q | S | E | T | S | L | Cytosol |
| Q3UU96 | MRCKa | S1629 | S1616 | P | G | R | S | M | S | A | S | S | G | Cytosol |
| Q8CH77 | NAV1 | S364 | S367 | P | M | R | S | P | S | K | L | S | H | Cytosol |
| P97434 | MPRIP | S993 | S992 | I | M | K | S | K | S | N | P | D | F | Cytosol |
| Q8C0T5 | SPAR1 | T9 | T9 | L | K | R | S | Q | T | E | R | P | V | Membrane, cytosol |
| Q9QYY0 | GAB1 | T387 | T388 | P | S | R | S | N | T | I | S | T | V | Cytosol |
| Q9CY57 | CHTOP | T15 | T15 | V | L | K | S | T | T | K | M | S | L | Nucleus |
| Q80YA9 | CNKR2 | T327 | T327 | I | P | R | S | P | T | S | S | V | A | Membrane, cytosol |
| Q8CGC4 | LSM14B | S181 | S181 | P | S | K | V | T | S | A | T | Q | L | Cytosol |
| P47963 | RL13 | S106 | S106 | R | R | R | N | K | S | T | E | S | L | Cytosol |
| Q8CGZ0 | CHERP | S902 | S911 | Y | R | R | N | K | S | Y | S | F | I | Nucleus, cytosol |
| P80318 | TCPG | S252 | S252 | Y | K | K | G | E | S | Q | T | D | I | Cytosol |
| Q80TH2 | Erbin | S1158 | S1150 | P | E | R | T | M | S | V | S | D | F | Nucleus, cytosol |

**Figure 3**

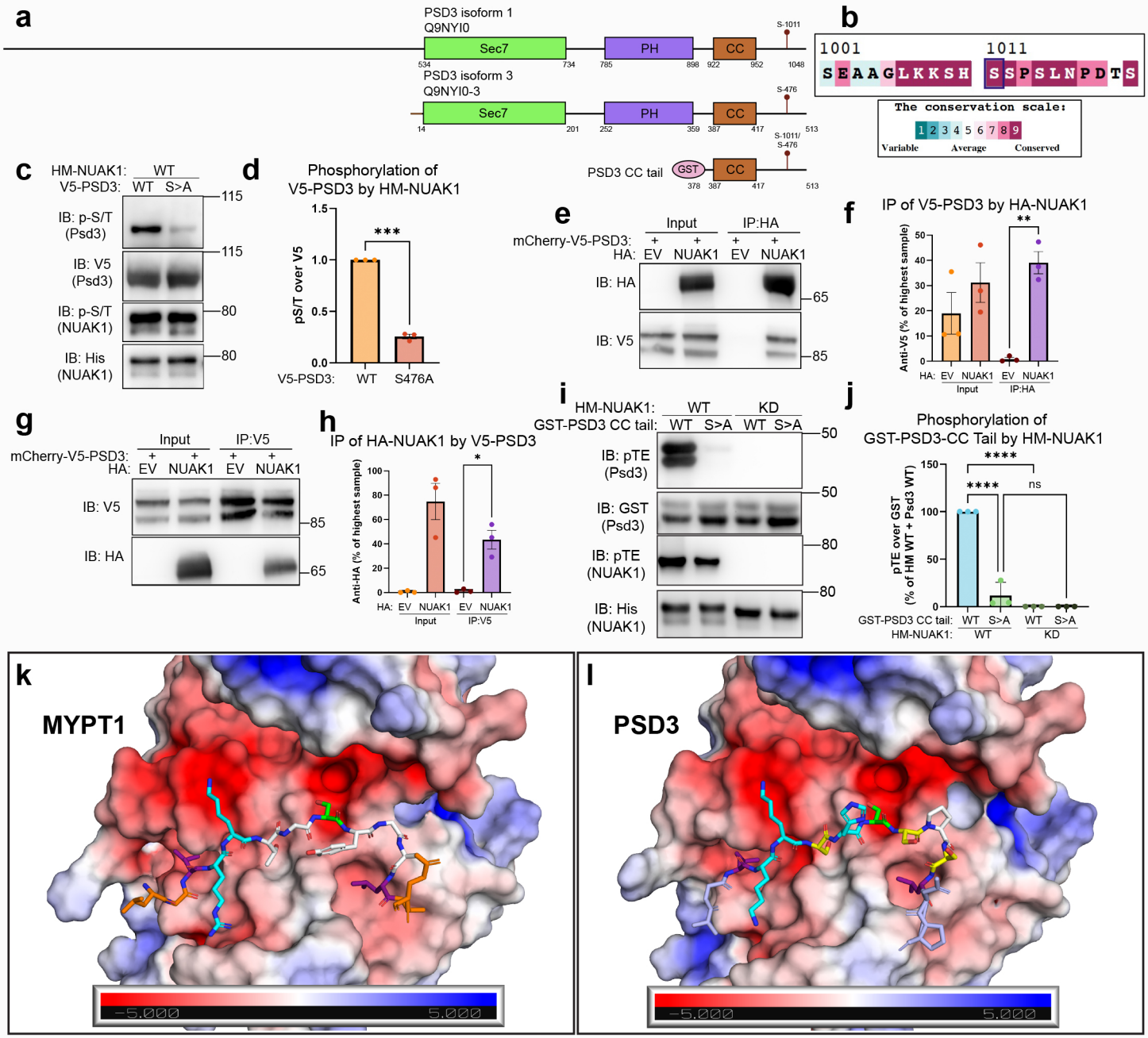
a
PSD3 isoform 1
Q9NYI0
Sec7
PH
CC
S-1011
534
734
785
898
922
952
1048
PSD3 isoform 3
Q9NYI0-3
S-476
14
201
252
359
387
417
513
S-1011/
S-476
PSD3 CC tail
GST
b
1001
1011
S E A A G L K K S H S S P S L N P D T S
The conservation scale:
1 2 3 4 5 6 7 8 9
Variable
Average
Conserved
c
HM-NUAK1: WT
V5-PSD3: WT S>A
IB: p-S/T (Psd3)
IB: V5 (Psd3)
IB: p-S/T (NUAK1)
IB: His (NUAK1)
115
115
80
80
d
Phosphorylation of V5-PSD3 by HM-NUAK1
pS/T over V5
***
V5-PSD3: WT S476A
e
Input
IP:HA
mCherry-V5-PSD3:
HA: EV NUAK1 EV NUAK1
IB: HA
IB: V5
65
85
f
IP of V5-PSD3 by HA-NUAK1
Anti-V5 (% of highest sample)
**
HA: EV NUAK1 EV NUAK1
Input
IP:HA
g
Input
IP:V5
mCherry-V5-PSD3:
HA: EV NUAK1 EV NUAK1
IB: V5
IB: HA
85
65
h
IP of HA-NUAK1 by V5-PSD3
Anti-HA (% of highest sample)
*
HA: EV NUAK1 EV NUAK1
Input
IP:V5
i
HM-NUAK1: WT KD
GST-PSD3 CC tail: WT S>A WT S>A
IB: pTE (Psd3)
IB: GST (Psd3)
IB: pTE (NUAK1)
IB: His (NUAK1)
50
50
80
80
j
Phosphorylation of GST-PSD3-CC Tail by HM-NUAK1
pTE over GST (% of HM WT + Psd3 WT)
****
****
ns
GST-PSD3 CC tail: WT S>A WT S>A
HM-NUAK1: WT KD
k
MYPT1
-5.000
5.000
l
PSD3
-5.000
5.000

Figure 4

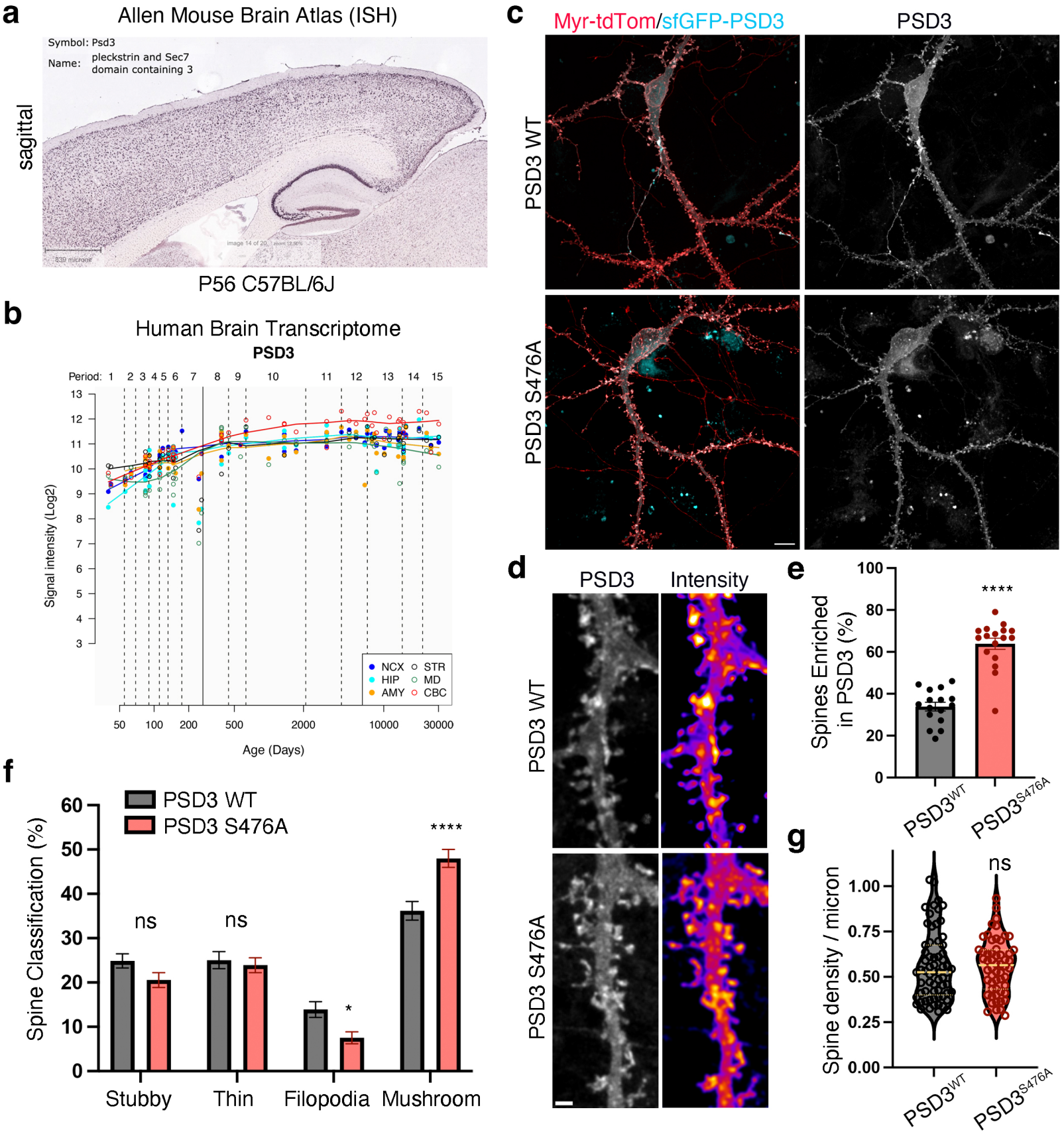
a
Allen Mouse Brain Atlas (ISH)
Symbol: Psd3
Name: pleckstrin and Sec7 domain containing 3
sagittal
P56 C57BL/6J
b
Human Brain Transcriptome
PSD3
Period: 1 2 3 4 5 6 7 8 9 10 11 12 13 14 15
Signal intensity (Log2)
Age (Days)
NCX
HIP
AMY
STR
MD
CBC
c
Myr-tdTom/sfGFP-PSD3
PSD3
PSD3 WT
PSD3 S476A
d
PSD3
Intensity
PSD3 WT
PSD3 S476A
e
Spines Enriched in PSD3 (%)
****
PSD3WT
PSD3S476A
f
PSD3 WT
PSD3 S476A
Spine Classification (%)
ns
ns
*
****
Stubby
Thin
Filopodia
Mushroom
g
Spine density / micron
ns
PSD3WT
PSD3S476A

**Figure 5**

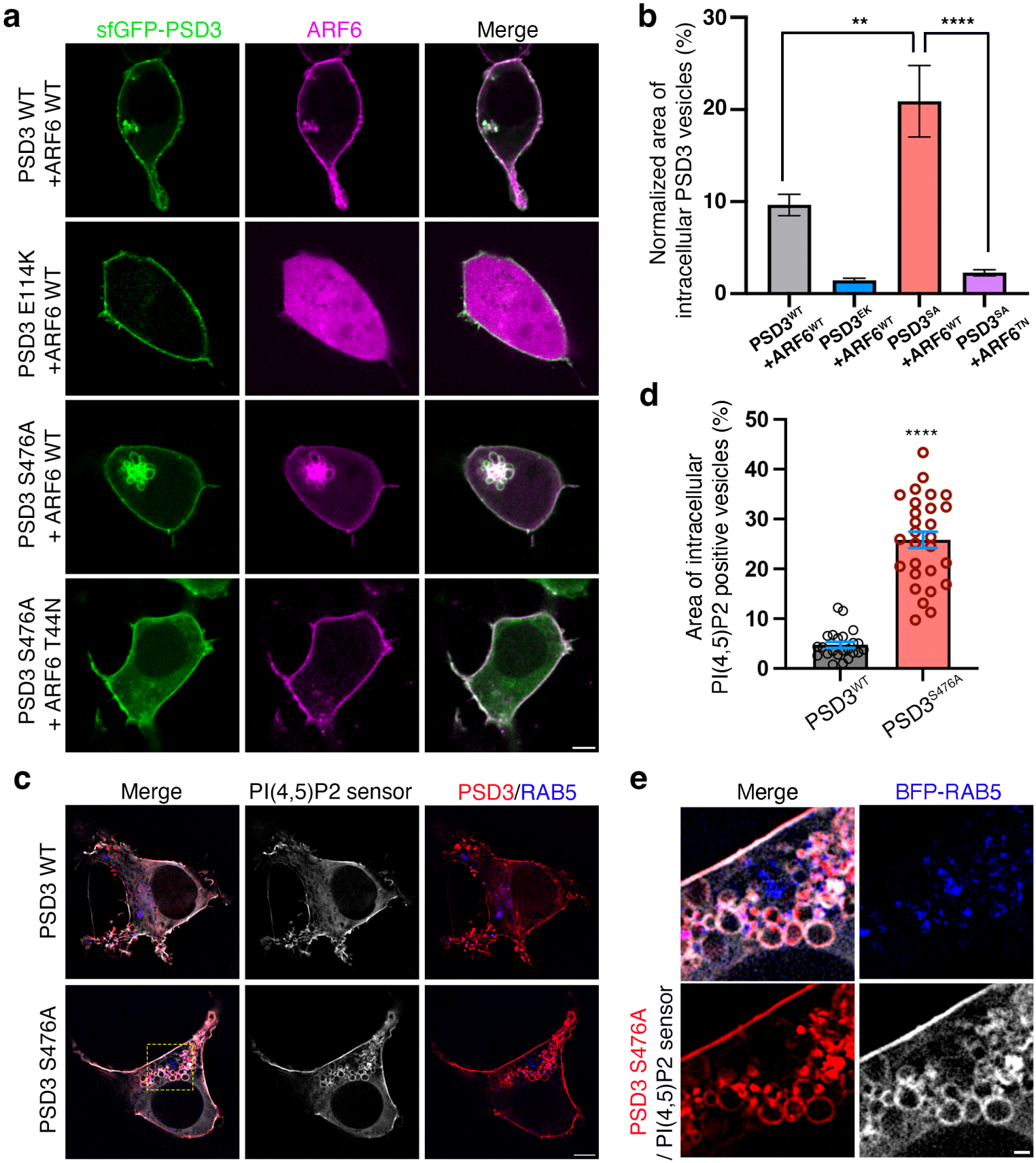
a
sfGFP-PSD3
ARF6
Merge
PSD3 WT +ARF6 WT
PSD3 E114K +ARF6 WT
PSD3 S476A + ARF6 WT
PSD3 S476A + ARF6 T44N
b
Normalized area of intracellular PSD3 vesicles (%)
30
20
10
0
**
****
PSD3WT +ARF6WT
PSD3EK +ARF6WT
PSD3SA +ARF6WT
PSD3SA +ARF6TN
d
Area of intracellular PI(4,5)P2 positive vesicles (%)
50
40
30
20
10
0
****
PSD3WT
PSD3S476A
c
Merge
PI(4,5)P2 sensor
PSD3/RAB5
PSD3 WT
PSD3 S476A
e
Merge
BFP-RAB5
PSD3 S476A / PI(4,5)P2 sensor

**Figure 6**

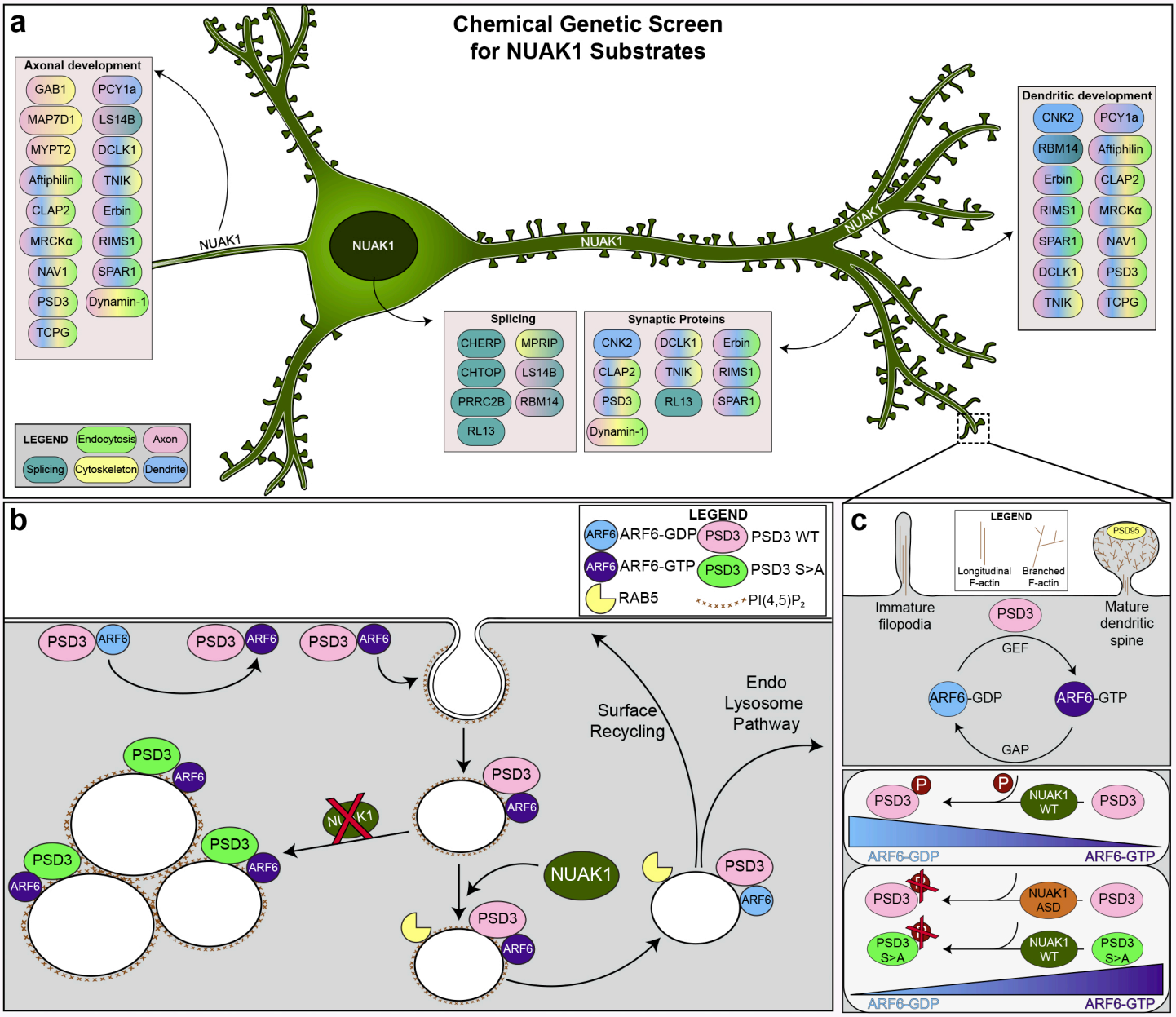
a
Chemical Genetic Screen
for NUAK1 Substrates
Axonal development
GAB1
PCY1a
MAP7D1
LS14B
MYPT2
DCLK1
Aftiphilin
TNIK
CLAP2
Erbin
MRCKα
RIMS1
NAV1
SPAR1
PSD3
Dynamin-1
TCPG
NUAK1
NUAK1
NUAK1
NUAK1
Dendritic development
CNK2
PCY1a
RBM14
Aftiphilin
Erbin
CLAP2
RIMS1
MRCKα
SPAR1
NAV1
DCLK1
PSD3
TNIK
TCPG
Splicing
CHERP
MPRIP
CHTOP
LS14B
PRRC2B
RBM14
RL13
Synaptic Proteins
CNK2
DCLK1
Erbin
CLAP2
TNIK
RIMS1
PSD3
RL13
SPAR1
Dynamin-1
LEGEND
Endocytosis
Axon
Splicing
Cytoskeleton
Dendrite
b
LEGEND
ARF6 ARF6-GDP
PSD3 PSD3 WT
ARF6 ARF6-GTP
PSD3 PSD3 S>A
RAB5
PI(4,5)P2
PSD3
ARF6
Surface
Recycling
Endo
Lysosome
Pathway
NUAK1
c
LEGEND
Longitudinal
F-actin
Branched
F-actin
PSD95
Immature
filopodia
Mature
dendritic
spine
PSD3
GEF
ARF6-GDP
ARF6-GTP
GAP
P
NUAK1
WT
ARF6-GDP
ARF6-GTP
NUAK1
ASD
PSD3
S>A
NUAK1
WT
PSD3
S>A
ARF6-GDP
ARF6-GTP

Figure 7

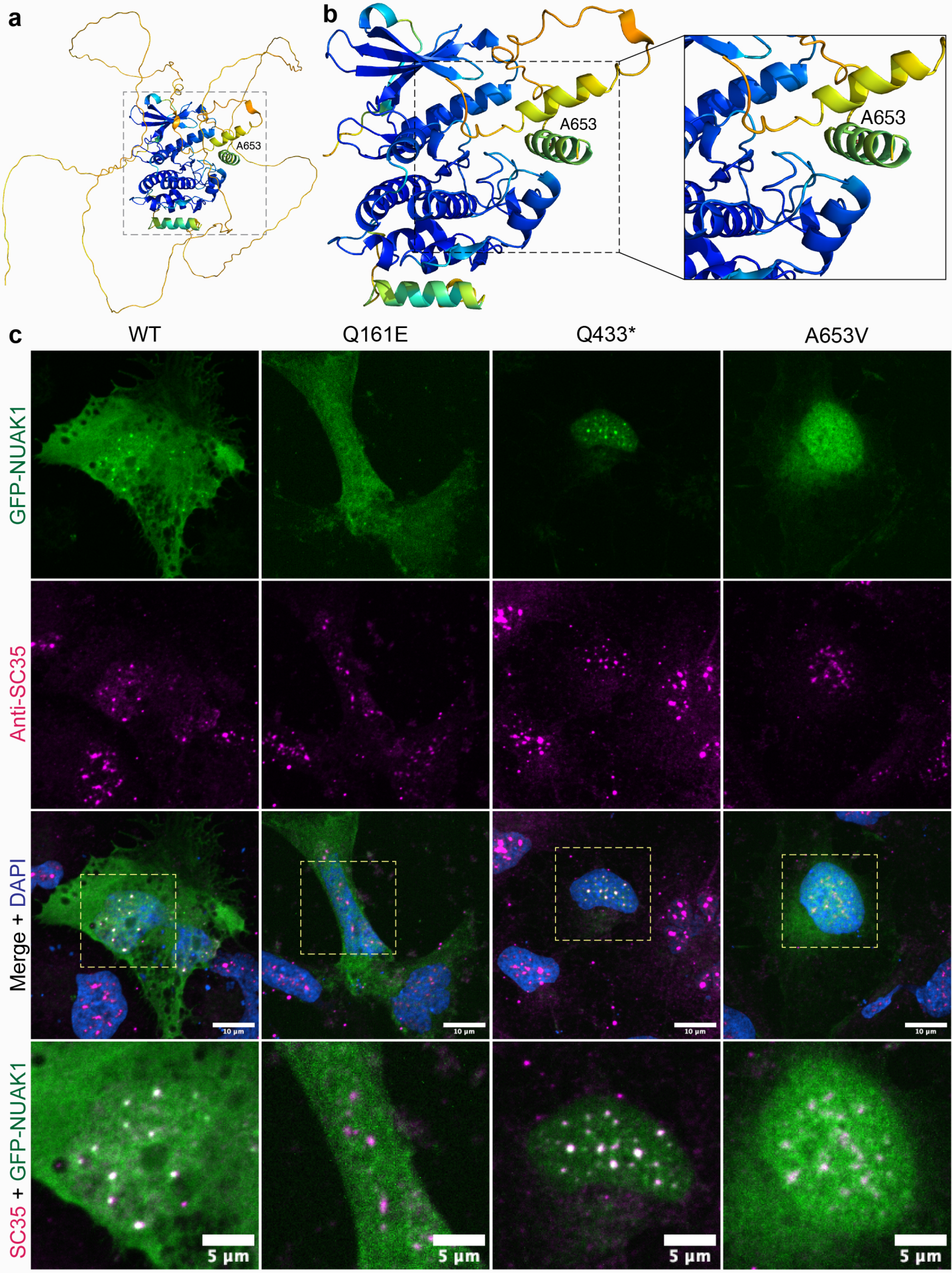
a
A653
b
A653
A653
c
WT
Q161E
Q433*
A653V
GFP-NUAK1
Anti-SC35
Merge + DAPI
SC35 + GFP-NUAK1
10 µm
5 µm

**Figure S1**

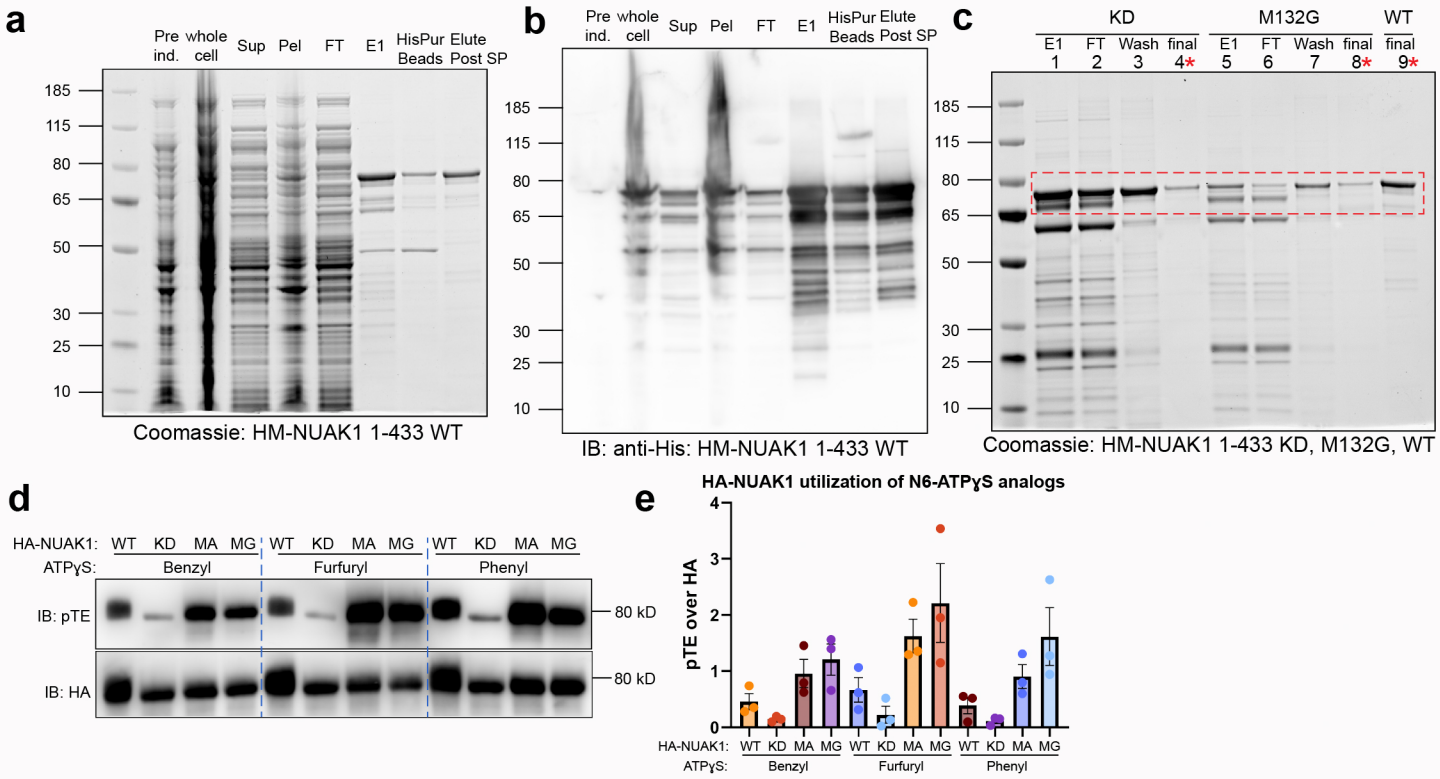
a
Pre ind.
whole cell
Sup
Pel
FT
E1
HisPur Beads
Elute Post SP
185
115
80
65
50
30
25
10
Coomassie: HM-NUAK1 1-433 WT
b
IB: anti-His: HM-NUAK1 1-433 WT
c
KD
M132G
WT
E1 1
FT 2
Wash 3
final 4*
E1 5
FT 6
Wash 7
final 8*
final 9*
Coomassie: HM-NUAK1 1-433 KD, M132G, WT
d
HA-NUAK1: WT KD MA MG WT KD MA MG WT KD MA MG
ATPγS: Benzyl Furfuryl Phenyl
IB: pTE
IB: HA
80 kD
80 kD
e
HA-NUAK1 utilization of N6-ATPγS analogs
pTE over HA
0
1
2
3
4
HA-NUAK1: WT KD MA MG WT KD MA MG WT KD MA MG
ATPγS: Benzyl Furfuryl Phenyl

# Figure S2

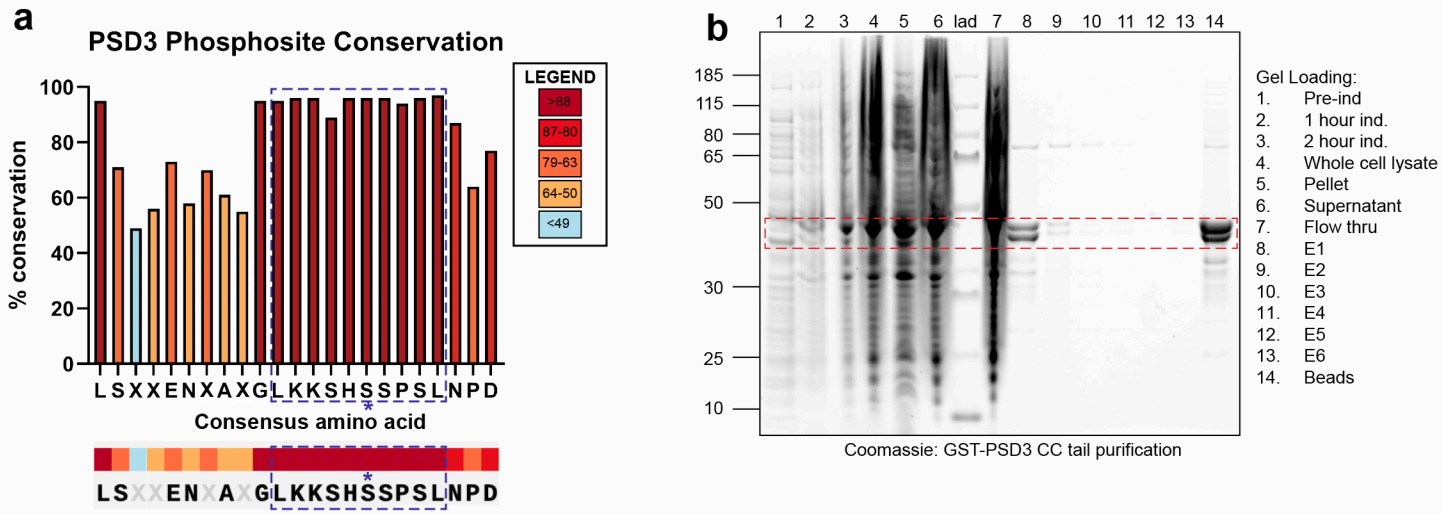
a
PSD3 Phosphosite Conservation
% conservation
100
80
60
40
20
0
L S X X E N X A X G L K K S H S S P S L N P D
Consensus amino acid
LEGEND
>88
87-80
79-63
64-50
<49
b
1 2 3 4 5 6 lad 7 8 9 10 11 12 13 14
185
115
80
65
50
30
25
10
Gel Loading:
1. Pre-ind
2. 1 hour ind.
3. 2 hour ind.
4. Whole cell lysate
5. Pellet
6. Supernatant
7. Flow thru
8. E1
9. E2
10. E3
11. E4
12. E5
13. E6
14. Beads
Coomassie: GST-PSD3 CC tail purification

# Figure S3